

THE PLANETARY MASS COMPANION 2MASS 1207–3932B: TEMPERATURE, MASS, AND EVIDENCE FOR AN EDGE-ON DISK

SUBHANJOY MOHANTY,¹ RAY JAYAWARDHANA,² NURIA HUÉLAMO,³ AND ERIC MAMAJEK¹

Received 2006 April 8; accepted 2006 October 10

ABSTRACT

We present *J*-band imaging and *H+K*-band low-resolution spectroscopy of 2MASS 1207–3932AB, obtained with VLT NACO. For the putative planetary mass secondary, we find $J = 20.0 \pm 0.2$ mag. The *HK* spectra of both components imply low gravity and a dusty atmosphere for the secondary. Comparisons to synthetic spectra yield $T_{\text{eff},A} \approx 2550 \pm 150$ K and $T_{\text{eff},B} \approx 1600 \pm 100$ K, consistent with their late-M and mid- to late-L types. For these T_{eff} and an age of 5–10 Myr, evolutionary models imply $M_A \approx 24 \pm 6 M_{\text{Jup}}$ and $M_B \approx 8 \pm 2 M_{\text{Jup}}$. Independent comparisons of these models to the observed colors, spanning $\sim I$ to L' , also yield the same masses and temperatures. Our primary mass agrees with other recent analyses; however, our secondary mass, while still in the planetary regime, is 2–3 times larger than claimed previously. This discrepancy can be traced to the luminosities: while the absolute photometry and M_{bol} of the primary agree with theoretical predictions, the secondary is $\sim 2.5 \pm 0.5$ mag fainter than expected in all bands from I to L' and in M_{bol} . This accounts for the much lower secondary mass (and temperature) derived earlier. We argue that this effect is highly unlikely to result from a variety of model-related problems and is instead real. This conclusion is bolstered by the absence of any luminosity problems in either the primary or AB Pic B, which we also analyze. We therefore suggest gray extinction in 2M1207B, due to occlusion by an edge-on circumsecondary disk. This is consistent with the observed properties of edge-on disks around T Tauri stars and with the known presence of a high-inclination evolved disk around the primary. Finally, the system’s implied mass ratio of ~ 0.3 suggests a binary-like formation scenario.

Subject headings: circumstellar matter — planetary systems — stars: formation — stars: low-mass, brown dwarfs — stars: pre-main-sequence — techniques: spectroscopic

1. INTRODUCTION

The nearby young brown dwarf 2MASS J1207334–393254 (hereafter 2M1207A) has been the subject of widespread attention in recent years. Based on its location, proper motion, and spectral signatures of youth, Gizis (2002) proposed that it is a likely member of the ~ 8 Myr old TW Hydreae association (henceforth TWA), one of the closest known young clusters (~ 50 pc). His low-resolution optical spectrum also evinced strong $\text{H}\alpha$ emission, possibly indicative of disk accretion. High-resolution optical spectra subsequently obtained by Mohanty et al. (2003) showed the $\text{H}\alpha$ emission profile to be broad, asymmetric, and variable over timescales of hours and also revealed strong emission in many other Balmer lines and in He I. These characteristics greatly bolstered the case for ongoing accretion. Mohanty et al. (2003) further derived radial and rotational velocities for 2M1207A and showed the radial velocity to be congruent with that expected of a TWA member. Finally, the X-ray versus $\text{H}\alpha$ analysis by Gizis & Bharat (2004) provided additional support for ongoing disk accretion in 2M1207A.

Mohanty et al. (2005) subsequently calculated an accretion rate of approximately $< 10^{-11} M_{\odot} \text{ yr}^{-1}$. More recently, Scholz et al. (2005) and Scholz & Jayawardhana (2006) have found dramatic changes in the shape and intensity of 2M1207A’s $\text{H}\alpha$ profile over timescales ranging from hours to weeks, indicating variations in the accretion rate by a factor of 5–10 over ~ 6 weeks

(with the lower rates comparable to the value of Mohanty et al. 2005). These authors have also identified a redshifted absorption component in $\text{H}\alpha$, quasi-periodic over day-long timescales. The presence of this component indicates asymmetric, magnetically channeled accretion columns rising from the surrounding disk; furthermore, its ~ 1 day periodicity, compared to the $v \sin i$ found by Mohanty et al. (2003) and the expected radii of young brown dwarfs, suggests that the disk is viewed at a high inclination angle (i.e., relatively close to edge-on: $i \gtrsim 60^\circ$).

Jayawardhana et al. (2003) did not find any L' -band ($3.8 \mu\text{m}$) excess disk emission from 2M1207A. However, Sterzik et al. (2004) detected ~ 8 – $11 \mu\text{m}$ mid-infrared excess from the disk, a situation similar to two other stellar members of TWA (Jayawardhana et al. 1999). Gizis et al. (2005a) have recently detected the disk out to $24 \mu\text{m}$ with *Spitzer*. The shape of the mid-IR spectral energy distribution (SED), combined with the lack of $10 \mu\text{m}$ silicate emission (Sterzik et al. 2004), suggests that the dust disk is flat, with significant grain growth and/or settling. Warm disk gas has now also been seen around 2M1207A, via the detection of fluorescent H_2 emission (Gizis et al. 2005b). Together, all of these data establish 2M1207A as the *closest known young brown dwarf with a surrounding accretion disk*.

Meanwhile, Chauvin et al. (2004) announced the direct detection of a possibly planetary mass companion to 2M1207A, at a projected separation of $\sim 0.78''$. Their HK, L' photometry suggested a spectral type of $\sim L5$ – $L9.5$ for the secondary, and their *H*-band low-resolution spectrum, while quite poor in signal-to-noise ratio (S/N), appeared consistent with this estimate. *Hubble Space Telescope (HST)* NICMOS photometry by Song et al. (2006), covering roughly I to H bands, also indicates a similar spectral type (mid to late L). Assuming a distance of ~ 70 pc, Chauvin et al. (2004) derived a luminosity for the secondary;

¹ Harvard-Smithsonian Center for Astrophysics, Cambridge, MA; smohanty@cfa.harvard.edu, emamajek@cfa.harvard.edu.

² Department of Astronomy and Astrophysics, University of Toronto, Toronto, ON, Canada; rayjay@astro.utoronto.ca.

³ Very Large Telescope, European Southern Observatory, Chile; nhuelamo@eso.org.

adopting an age of ~ 8 Myr and comparing to age-luminosity evolutionary models, they then arrived at a mass of $\sim 5M_{\text{Jup}}$ and effective temperature (T_{eff}) of ~ 1250 K. The following year, Chauvin et al. (2005a) presented astrometric observations that strongly supported the physical association of the primary (2M1207A) and secondary (2M1207B); the two almost certainly form a single, bound, comoving system.

Subsequently, Mamajek (2005), with refined space motions for 2M1207A and TWA combined with a detailed moving cluster analysis, showed that (1) 2M1207A is indeed a bona fide member of TWA and (2) its distance is 53 ± 6 pc, in agreement with the known distances to other TWA members and significantly less than the 70 pc assumed by Chauvin et al. (2004, 2005a). Song et al. (2006) have also arrived at a very similar distance, using a scaled proper-motion technique: 59 ± 7 pc, within 1σ of the Mamajek (2005) value and again lower than the Chauvin et al. (2004, 2005a) estimate. The reduction in distance decreases the estimated luminosity of 2M1207B and thus lowers its inferred mass: employing his new distance, but otherwise carrying out exactly the same age-luminosity analysis as Chauvin et al. (2004), Mamajek (2005) derived a mass of just $3\text{--}4 M_{\text{Jup}}$ for the secondary. While Mamajek (2005) did not state what T_{eff} this mass corresponds to, the evolutionary models he uses (Chabrier et al. 2000; Baraffe et al. 2003) indicate $T_{\text{eff}} \sim 900\text{--}1050$ K, at the adopted age of ~ 8 Myr.

2M1207B is thus unique in several respects: it is the coolest known confirmed substellar object at an age of a few Myr; if the above mass estimates are valid, it is also arguably the first directly imaged planetary mass companion outside the solar system (and certainly the first imaged one with confirmation of common proper motion) and the first such body discovered around a brown dwarf. From the point of view of substellar binary systems too, 2M1207AB is quite remarkable. On the one hand, given the high multiplicity frequency among low-mass stars in TWA (Brandeker et al. 2003), it is perhaps not surprising to find a substellar binary like 2M1207AB. However, brown dwarf binaries wider than 20 AU appear to be absent in older (~ 100 Myr old) open clusters (e.g., Martín et al. 2003; Bouy et al. 2006b), as well as in the nearby field (Bouy et al. 2003; Burgasser et al. 2003a). In very young ($\sim 1\text{--}5$ Myr old) star-forming regions too, the substellar binary separation seems comparable to that in the field (Kraus et al. 2005, 2006; although there is a hint that some wider brown dwarf binaries may exist at such ages; Bouy et al. 2006a; Luhman 2004). With a separation of at least ~ 40 AU (using the projected angular separation and the Mamajek [2005] distance), the ~ 8 Myr old 2M1207AB system is definitely an outlier compared to these results and can potentially illuminate evolutionary and/or environmental effects on substellar binarity. In short, 2M1207B offers critical insights into the properties of ultracool objects at young ages, the origin of planetary mass companions, the formation of substellar bodies in general, and binarity in the brown dwarf domain.

2. SPECTRAL TYPE VERSUS TEMPERATURE DISCREPANCY IN EARLIER ANALYSES

However, one fundamental aspect of 2M1207B's inferred properties is rather troubling. The $T_{\text{eff}} \sim 1250$ K derived by Chauvin et al. (2004), based ultimately on an overlarge distance, corresponds in the field to early-T dwarfs (Golimowski et al. 2004). The $\sim 900\text{--}1050$ K implied by Mamajek's (2005) analysis, based on a more rigorous distance estimate, corresponds to mid-to late-T dwarfs. Finally, the $T_{\text{eff}} \sim 1250$ K derived by Song et al. (2006) from *HST* absolute photometry down to $\sim I$ again corre-

sponds, like the Chauvin et al. (2004) estimate, to early-T dwarfs. Thus, at least compared to field dwarfs, even the Chauvin et al. (2004) and Song et al. (2006) T_{eff} is at odds with the mid- to late-L type they themselves observe for 2M1207B, while the T_{eff} suggested by Mamajek's (2005) analysis is entirely inconsistent with this spectral type. Specifically, the settling of photospheric dust and the appearance of CH_4 absorption in the K band already make early-T dwarfs *bluer* in $H - K$ than hotter, earlier spectral types, while mid- to late-T dwarfs are severely bluer (e.g., Knapp et al. 2004). In contrast, Chauvin et al. (2004) show that 2M1207B is extremely *red* in $H - K$ (which is why they derive a mid- to late-L type in the first place), suggesting a significantly higher T_{eff} than inferred from their luminosity analyses or those of Song et al. (2006) or Mamajek (2005). In short, there seems to be a serious discrepancy between the T_{eff} implied for 2M1207B by its estimated luminosity and the T_{eff} suggested by its observed spectral type.

Of course, 2M1207B is much younger than field dwarfs, so this apparent discrepancy may be due to its much lower gravity. Either way, given the importance of this object, the mismatch is worth investigating in detail. To this end, we have obtained J -band photometry and HK -band low-resolution spectroscopy of both 2M1207A and 2M1207B on the European Southern Observatory's Very Large Telescope (VLT) and compared our data (along with previous photometry) to the latest synthetic spectra and evolutionary models. Our spectral and color analyses directly yield temperature and mass estimates, independent of luminosity. The T_{eff} we derive for both bodies are consistent with their previously cited spectral types. In particular, the T_{eff} implied by 2M1207B's SED is substantially higher than suggested by the Chauvin et al. (2004), Song et al. (2006), and Mamajek (2005) luminosity considerations, as suspected a priori from the spectral type deliberations above. Low gravity alone cannot resolve this discrepancy. Instead, it appears that 2M1207B is anomalously underluminous, due to gray extinction in the infrared. We support this conclusion by showing that the recently discovered young brown dwarf AB Pic B (Chauvin et al. 2005b), which is roughly similar to 2M1207B in temperature, spectral type, and age, does *not* exhibit any temperature-luminosity discrepancies: 2M1207B is indeed peculiarly faint. We ascribe this to the presence of a nearly edge-on disk around 2M1207B. Our mass for 2M1207B is also correspondingly higher (although still in the planetary regime), supporting the idea that the 2M1207AB system formed in a manner analogous to stellar binaries.

All our results are tabulated in Table 1.

3. OBSERVATIONS

J -band imaging and $H+K$ -band low-resolution spectroscopy of 2M1207A and 2M1207B were performed on ESO's VLT in Chile, using the Near-infrared Adaptive Optics System (NAOS) with the infrared camera and spectrometer CONICA (NACO). Wave front sensing was in the near-infrared (NIR), guiding on the primary (2M1207A). The N90C10 dichroic (which sends 90% of the light to the wave front sensor and 10% to the science camera), High Sensitivity detector mode, and Fowler Nsample readout mode were employed throughout. Observations were in Service Mode and constrained to target air mass < 1.2 and visual seeing (before AO correction) $\lesssim 0.6''$.

The J -band images were acquired on 2005 March 26, with the CONICA S27 camera (pixel scale ≈ 27 mas pixel $^{-1}$, FOV = $28'' \times 28''$). A total of 80 images were taken, each of duration 30 s, yielding a total integration time of 40 minutes.

The $H+K$ -band low-resolution spectroscopy was carried out over the period 2005 April–June, with the HK filter (simultaneous

TABLE 1
OBSERVED AND DERIVED PROPERTIES OF 2MASS 1207–3932A AND 2MASS 1207–3932B

Name	$J_{\text{2MASS}}^{\text{a}}$ (mag)	$H_{\text{2MASS}}^{\text{b}}$ (mag)	$K_{s,\text{2MASS}}^{\text{b}}$ (mag)	L^{b} (mag)	Separation ^a (mag)	P.A. ^a (deg)	Spectral Type ^a	Distance ^c (pc)	Age ^b (Myr)	$\log(L/L_{\odot})^{\text{c}}$	$T_{\text{eff}}^{\text{a}}$ (K)	Mass ^a
2MASS 1207A	13.00 ± 0.03	12.39 ± 0.03	11.95 ± 0.03	11.38 ± 0.10	M8	53 ± 6	5–10	-2.68 ± 0.12	2550 ± 150	$20M_{\text{J}}\text{--}30M_{\text{J}}$
2MASS 1207B.....	20.0 ± 0.2	18.09 ± 0.21	16.93 ± 0.11	15.28 ± 0.14	769 ± 10	125.6 ± 0.7	Mid to late L	-4.72 ± 0.14	1600 ± 100	$6M_{\text{J}}\text{--}10M_{\text{J}}$

^a This work.

^b Chauvin et al. (2004).

^c Mamajek (2005).

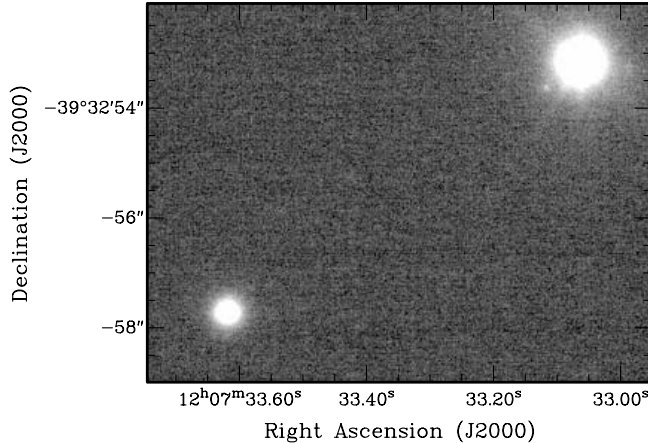


FIG. 1.—Our final reduced J -band image, showing the 2M1207AB system in the upper right corner (the secondary is visible near the lower left rim of the primary) and a background K-type giant in the lower left corner. North is up, east is left; the separation between 2M1207A and the K giant is $\sim 7''$.

coverage over H and K bands, $1.3\text{--}2.6\ \mu\text{m}$), a slit width of 86 mas, and the S54 camera (pixel scale ≈ 54 mas pixel $^{-1}$, FOV = $56'' \times 56''$). The spectral resolution was ~ 550 . A total of 31 spectra were obtained, in four observing blocks (OBs) of eight spectra each (except for one 2005 June OB, in which seven spectra were taken instead of eight; see below); exposure time for each frame was 300 s, giving a total integration time of 155 minutes.

The eight spectra in each OB were taken in an “abbaabba” nod cycle, i.e., as four pairs of spectra at two nod positions each. The slit was oriented along the 2M1207A-B axis, with nodding along the slit, yielding simultaneous spectra of both components at each nod. A glitch terminated the first OB of 2005 June 3 after only seven nods, before the last spectrum in the cycle was taken; a second complete block of eight spectra was therefore obtained on the same night. Subsequent examination showed the seven spectra from the first OB to be perfectly viable as well, and they are included in our analysis along with all of the other spectra.

Finally, we also use previously published photometry of 2M1207 in our analysis: ground-based J , H , K_s , L' for the primary (2MASS All Sky Catalog of Point Sources; Cutri et al. 2003; Jayawardhana et al. 2003) and H , K_s , L' for the secondary (Chauvin et al. 2004).

4. DATA REDUCTION

4.1. Photometry

The J -band images were flat-fielded, registered, and co-added using the NACO pipeline reduction software ECLIPSE (Devillard 1997). 2M1207A and 2M1207B are clearly visible as separate sources; a background K-type star is also visible southeast of the 2M1207 system (Figs. 1 and 2). Apparent J magnitudes for both 2M1207A and the K-type star are available in the 2MASS database.⁴ The J magnitude of 2M1207B was determined through relative photometry with respect to 2M1207A; we checked the validity of our flux calculations by similarly deriving the J magnitude of the K-type star as well, relative to 2M1207A, and comparing to its 2MASS value.

Background-subtracted counts (in arbitrary units) for 2M1207A and the K-type star were determined first, with the IRAF APPHOT

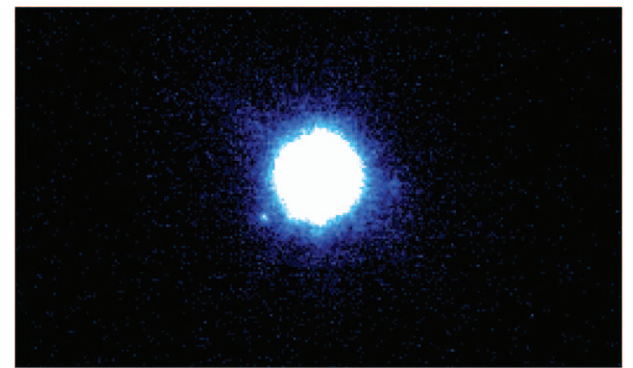


FIG. 2.—Zoom-in view of Fig. 1. North is up, east is left. 2M1207A is the central bright source, 2M1207B the bright dot to its immediate lower left, at a separation of 769 ± 10 mas and position angle (east of north) of $125.6^\circ \pm 0.7^\circ$.

package. Our errors in photometry are dominated by photon (shot) noise. While 2M1207B sits on the wings of the primary, its flux contribution relative to the primary is completely negligible ($\ll 1\%$; see below), and no attempt was made to exclude it while extracting the counts for 2M1207A. Adopting the 2MASS magnitude for 2M1207A ($J = 13.00 \pm 0.03$) and the magnitude difference between it and the (fainter) K-type star implied by our aperture photometry ($\Delta J = 2.32 \pm 0.01$) yields $J = 15.32 \pm 0.03$ for the latter. This agrees very well with the 2MASS magnitude for this source, $J = 15.39 \pm 0.07$, supporting the overall validity of our calculations.

Extracting the flux of 2M1207B alone requires more effort, given its proximity to the much brighter primary: we must first subtract the underlying contribution of the latter. A simple way of doing so is suggested by a contour plot of the 2M1207 point-spread function (PSF; Fig. 3, *left panel*), which reveals 2M1207A’s PSF to be very symmetric about the x -axis. We therefore reflect the co-added J image about the x -axis, drawn through the centroid of 2M1207A located by IRAF APPHOT, and subtract the reflected image from the original. The right panel of Figure 3 shows the residual contours after subtraction: the procedure clearly removes the primary’s contribution at the secondary’s position with high fidelity, leaving behind a clean image of 2M1207B on a flat, relatively null background. 2M1207B’s counts are extracted from this residual image after subtracting the remaining flat background, using APPHOT; the errors are dominated by photon noise. Relative photometry against 2M1207A yields $\Delta J = 7.0 \pm 0.2$; adopting the 2MASS value of $J = 13.00 \pm 0.03$ for the latter then implies $J = 20.0 \pm 0.2$ for 2M1207B. As a consistency check, the flux for 2M1207B was independently extracted for us by F. Marchis using the ADONIS deconvolution software; the cleaned image from this procedure was very similar to ours, and the resulting J -band photometry fully consistent with our value.

Note that our relative photometry implicitly assumes that the 2MASS and VLT filters are identical (as also assumed by Chauvin et al. [2004] for their H and K_s photometry of this system). Stephens & Leggett (2004) have shown that the infrared magnitudes of L and T dwarfs are very sensitive to the precise filter bandpass used; since 2M1207B has been previously classified as an L type, we have compared the VLT and 2MASS filters to check for any potential systematics in our photometry. We find that the JHK_s filters are very similar in the two systems: errors due to bandpass differences should be of order $\lesssim 0.1$ mag, smaller than the ± 0.2 mag uncertainty we already quote for our relative photometry.

⁴ While the 2MASS spatial resolution is too low to distinguish between 2M1207A and 2M1207B, 2M1207B alone is well below the survey’s detection limit, so the 2MASS fluxes for 2M1207 correspond to that of 2M1207A alone.

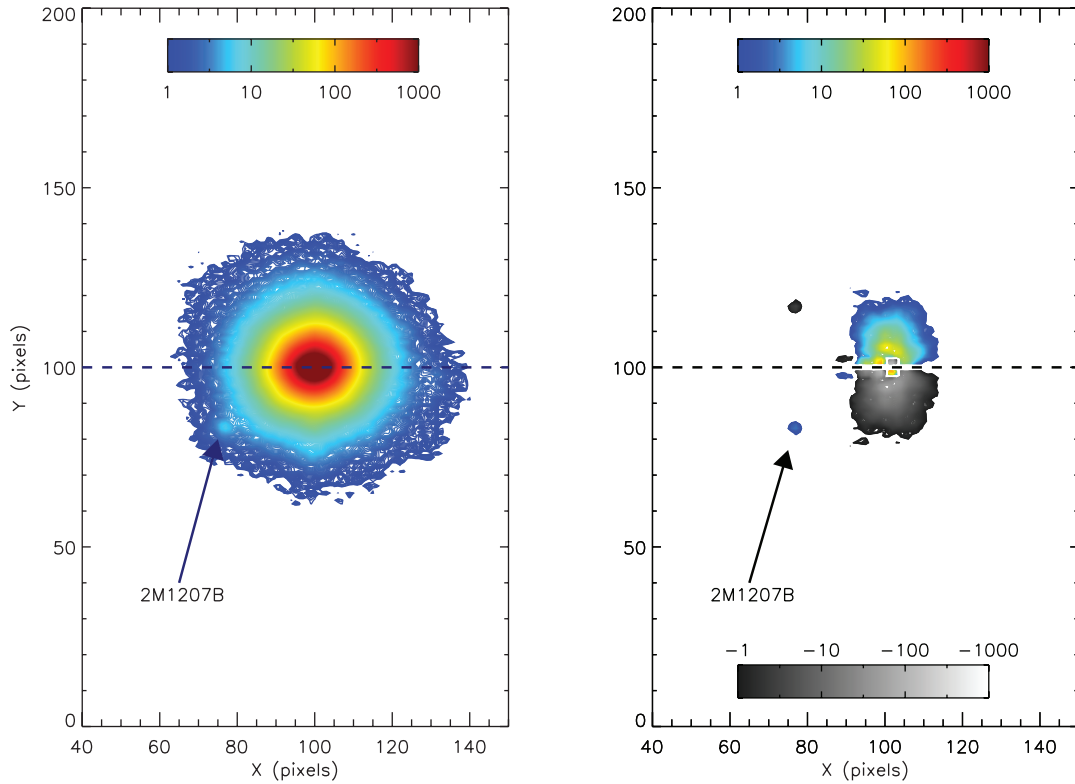


FIG. 3.—Contour plot illustration of our *J*-band photometry reduction procedure. *Left:* Contour plot of the combined PSFs of 2M1207A and 2M1207B, with observed counts (from +1 to +1000) in logarithmic units. The secondary, marked by an arrow, is visible as a faint source sitting on the wings of the primary. The primary's PSF is highly symmetric about the *X*-axis drawn through its centroid (*thick dashed line*). To extract the secondary, we reflect the primary's PSF about this axis and subtract from the original image. *Right:* Contour plot of the residuals after subtraction, in logarithmic units. Positive residuals (+1 to +1000) are shown in color, on the same scale as in the left panel, and negative residuals (-1 to -1000) are shown in gray scale. The residuals on either side of the *X*-axis are +ve and -ve mirror images. The procedure yields a clean image of the secondary (marked by arrow); residuals from the primary are <10% of the original counts everywhere.

4.2. Spectroscopy

The two-dimensional (2D) spectra within each spectroscopic OB were flat-fielded, background-subtracted by differencing each pair of nodded images, registered, and median-combined. A one-dimensional (1D) spectrum of 2M1207A for each OB was then extracted directly from this final median frame, using the *apall* task in IRAF.

For 2M1207B, the proximity of the primary demands a more sophisticated extraction procedure. While the PSF of the primary is very symmetric about the dispersion axis, self-subtraction after reflection about this axis (analogous to the technique described above for the *J*-band photometry; also employed by Close et al. [2005] for spectral extraction of AB Dor C) is not ideal for our purposes: the resulting 2M1207B spectrum is noisier than we would like in each wavelength bin.⁵ Instead, we model the PSF of the primary in detail, as described below.

As a first step toward increasing the S/N, we smooth the median 2D spectrum in each OB by a 5 pixel boxcar in the dispersion (*y*) direction; this correspondingly reduces our spectral resolution to ~ 100 . The spatial PSF of 2M1207A in each row (i.e., at each wavelength) of this smoothed image is then fitted by a sum of three Gaussians, plus a second-order polynomial (to account for any large-scale spatial background from chip QE ef-

fects), through a χ^2 minimization routine in IDL. During fitting, the pixels corresponding to the secondary's spectrum are assigned a weight of zero, so they do not contribute to the fit. The resulting image is our model 2D spectrum for 2M1207A. This is subtracted from the original smoothed image; the residual is a smoothed 2D spectrum of 2M1207B alone. The 1D spectrum of 2M1207B is then extracted from this residual image with IRAF *apall*.

Figure 4 illustrates the validity of this procedure. We display the original smoothed median 2D spectral image for a representative OB (2005 April 4), showing the combined spectra of 2M1207A and 2M1207B, our model fit to 2M1207A for this spectrum, and the residual spectrum of 2M1207B after model subtraction. The fit is very good in the vicinity of the secondary, and the subtraction produces a relatively clean secondary spectrum on a flat null background (apart from noise, nonzero residuals remain only near the peak of the primary, far from the secondary's position). As a second check on our extraction, we have compared the 2M1207B spectra obtained via this PSF fitting method to the spectra derived from the simple reflected image subtraction method mentioned earlier. While the fitting procedure produces much better S/N spectra, as expected, the general shape of the final spectrum is the same for both techniques, confirming the validity of our detailed fitting analysis.

The final result of all of the above steps is a set of four spectra each for 2M1207A and 2M1207B: one for each of our four spectroscopic OBs. The wavelength scale for each spectrum is derived from argon arc spectra. As mentioned earlier, the 2M1207A spectra have a resolution of ~ 550 , while the 2M1207B spectra have been smoothed during extraction to $R \sim 100$. These spectra are

⁵ The noise in the final residual image is always higher, in this procedure, than in the original data: the original noise at every pixel is added in quadrature to the noise at the symmetric pixel in the reflected image during subtraction. In our extraction of the secondary's *integrated J*-band flux for photometry, this increase in noise was not a serious concern; however, it is a significant effect for *spectral* extraction, where we want the flux in individual narrow wavelength bins.

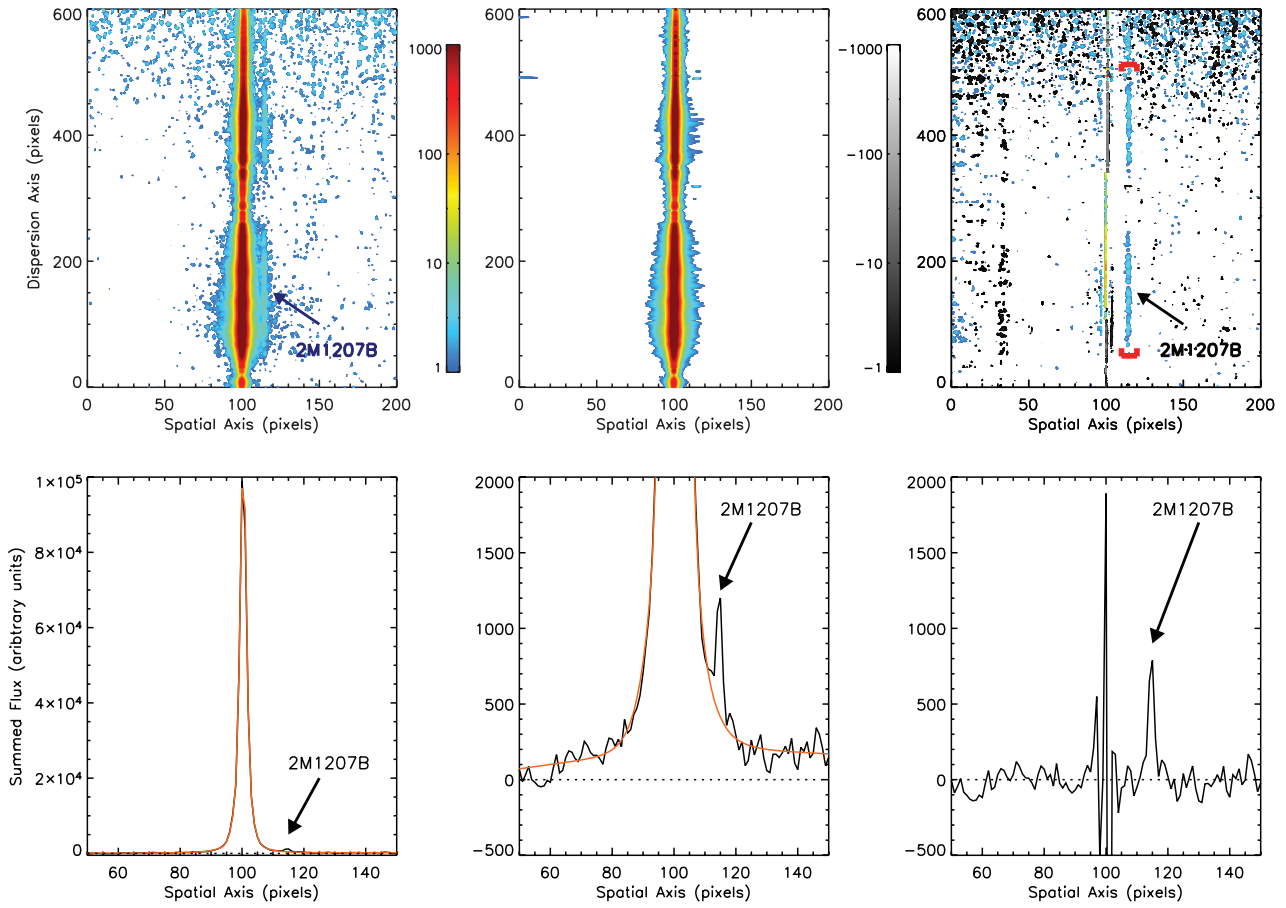


FIG. 4.—Illustration of our *HK* spectral reduction procedure, for a representative OB (from 2005 April 4). *Top left*: Contour plot of our original smoothed median 2D spectral image for this OB, with counts (from +1 to +1000) in logarithmic units. The central bright spectrum is that of the primary; the secondary is the faint strip on the right wing of the primary (marked by arrow). Wavelength increases along the *y*-axis, from bottom to top, with the *H* band in the bottom half and *K* band in the top half of the image. *Top middle*: Our model 2D spectrum for the primary (see § 4.2), on the same scale. *Top right*: Residuals, in logarithmic units, after subtracting model from original. Positive residuals (+1 to +1000) are shown in color, on the same scale as in the other two panels; negative residuals (−1 to −1000) are shown in gray scale. The procedure efficiently removes the primary (residuals everywhere are <10% of the original counts), leaving behind a clear spectrum of the secondary (marked by arrow). The red brackets indicate the region of the secondary’s spectrum we actually use in our subsequent analysis; the reddest parts of the *K* band are noisy and thus excluded. *Bottom panels*: Alternative representation of the same reduction. *Bottom left*: Spatial profile of our original 2D spectral image, after summing over dispersion axis. Central peak is 2M1207A; secondary marked by arrow. *Bottom middle*: Zoom-in of model spatial profile (red) overplotted on the data (black), showing an excellent fit to the primary, including in the vicinity of the secondary. *Bottom right*: Residual spatial profile after model subtraction, showing a clean profile of 2M1207B alone; primary residuals are <10% of the original counts everywhere and insignificant near the secondary.

dominated by telluric absorption bands and by the wavelength-dependent spectrograph response; these effects are removed with the help of telluric standards as follows.

Telluric standards were observed during each OB: HIP 073074 (G0 V; OB on 2005 April 4), HIP 059795 (G3 V; OB on 2005 April 30), and HIP 088409 (B3 III; both OBs on 2005 June 3). Two spectra were extracted, using *apall*, for each standard: one unsmoothed for correcting 2M1207A, and one smoothed by a 5 pixel boxcar, before extraction, for correcting 2M1207B. HIP 088409 is, moreover, slightly extincted, by $A_V \approx 1.0$ (revealed by our comparison to the colors of unreddened B3 stars and also cited by Rubin et al. 1962), producing a small change in the *HK* spectral slope; we have dereddened its spectrum accordingly. Next, narrow intrinsic spectral lines (e.g., Br γ absorption) in the telluric standards must be removed, to avoid producing spurious features in the science data on telluric correction. We accomplish this by dividing our telluric standard spectra by normalized (continuum divided out) spectra of appropriate spectral type standards, rebinned to our resolution. For HIP 073074 and HIP 059795, our spectral standard is a solar spectrum (G2 V; NSO/Kitt Peak FTS data, produced by NSF/NOAO and available on the VLT site); for

HIP 088409, we use a spectrum of HD 35653 (B0.5 V) from the NIR spectral library of Lançon & Rocca-Volmerange (1992). Finally, the intrinsic spectral slope of the telluric standards is removed by dividing by a blackbody of the appropriate T_{eff} : 5930, 5785, and 17,000 K for HIP 073074, HIP 059795, and HIP 088409, respectively. This leaves behind pure telluric absorption spectra, convolved with the wavelength-dependent spectrograph response. The 2M1207A and 2M1207B spectra are divided by these to produce the final telluric- and spectrograph response-corrected spectra for each OB.

The resulting *HK* spectra of 2M1207A from three of our four OBs are nearly identical and also agree very well with an *HK* spectrum of this source recently obtained with CORMASS on Magellan (K. Luhman 2005, private communication). The spectrum from the remaining OB (2005 April 4), however, shows a distinct linear change in slope compared to the other three. The spectrum of the secondary from the same OB also evinces an analogous slope offset relative to the others. Such an effect is expected from imperfect centering of the source in the narrow slit. Given the close agreement between three of our 2M1207A spectra and the independent CORMASS result, it is safe to assume that only the April 4 data

are anomalous. A linear slope correction factor is therefore derived for the April 4 2M1207A spectrum, by ratioing this spectrum with the median of the other three and fitting a straight line to the result. This correction factor is then applied to the April 4 spectra of both 2M1207A and 2M1207B.

Lastly, the spectra from the four OBs are normalized by their means over 2.1–2.2 μm and median-combined, producing one final spectrum each for 2M1207A and 2M1207B; these are the spectra used in our analysis. The S/N is ~ 30 for the primary and ~ 3 –10 for the secondary.

4.3. Astrometry

Our observations were designed for photometry and spectroscopy (the main topic of this paper) and not astrometry. Consequently, while the VLT provides nominal plate scale and plate rotation values for the CONICA S27 camera used for our *J*-band imaging, we have not obtained reference frames to estimate the errors in these quantities. Nevertheless, comparing them to the values found by Chauvin et al. (2004), from reference images with the same camera, lets us set conservative error bars as follows and still perform useful astrometry.

The nominal plate scale and plate rotation for CONICA S27 are 27.150 mas pixel $^{-1}$ and 0° (north up, east left), respectively. For the same camera, Chauvin et al. (2005a) cite a plate scale of 27.010 ± 0.05 mas pixel $^{-1}$ over their 1 yr of observations and a counterclockwise plate rotation of $0.07^\circ \pm 0.10^\circ$ to $0.14^\circ \pm 0.10^\circ$. For our calculations, therefore, we use the nominal S27 values but conservatively adopt error bars equal to the maximum difference between the Chauvin et al. (2005a) estimates for these parameters (including their error bars) and the nominal ones. That is, we use a plate scale of 27.150 ± 0.20 mas pixel $^{-1}$ and rotation of $0^\circ \pm 0.25^\circ$.

5. MODELS EMPLOYED: SYNTHETIC SPECTRA AND EVOLUTIONARY TRACKS

We compare the observed spectra to the latest synthetic spectra generated by the Lyon group with the PHOENIX code (Allard et al. 2001). Specifically, we use the models designated DUSTY-2000, COND-2002, and SETTL-2005 (Allard et al. 2001, 2003a⁶). These incorporate the most recent AMES line lists for both TiO (Langhoff 1997; Schwenke 1998) and H₂O (Partridge & Schwenke 1997). TiO opacity dominates in the optical, while H₂O dominates in the infrared. The models include about 500 million molecular lines (~ 307 million of H₂O and ~ 172 million of TiO), the formation of over 600 gas-phase species and 1000 liquids and crystals, and opacities of 30 different types of grains (Allard et al. 2000, 2001; although some important species remain absent: see § 7.1.3). All models used here are for solar metallicity ([M/H] = 0.0).

Convection in these models is handled with mixing-length theory (MLT), which seems to reasonably approximate the true convective transport mechanism (Chabrier & Baraffe 2000). The DUSTY-2000 models use $\alpha = 1.0$ (where $\alpha \equiv l/H_P$, with l being the mixing length and H_P the pressure scale height). However, recent full three-dimensional (3D) radiative hydrodynamical simulations indicate that $\alpha \approx 2$ is a better approximation for mid-M types, both in the field and in the pre-main-sequence phase (Ludwig 2003). Such simulations offer the best insight so far into the actual convection process (see Chabrier & Baraffe 2000); consequently, the COND-2002 and SETTL-2005 models, which

are more recent than DUSTY-2000, use $\alpha = 2$. In this context, we note that our TWA sources are expected to have an age ~ 5 –10 Myr and thus (according to theoretical evolutionary tracks) $\log g \approx 4 \pm 0.25$; the secondary is also expected to be very cool (< 2000 K) from the previous spectral type analysis by Chauvin et al. (2004). Baraffe et al. (2002) show that the value of α affects H₂ formation, and thus the evolutionary path (e.g., T_{eff} , L_{bol}), for extremely young (~ 1 Myr old), very low gravity ($\log g \leq 3.5$) objects with $T_{\text{eff}} \sim 2200$ –4000 K. However, they also show that the effect of α on evolution is negligible both by an age of ~ 10 Myr ($\log g > 3.5$) and for $T_{\text{eff}} < 2200$ K: at these higher gravities and/or lower T_{eff} , H₂ forms efficiently regardless of whether α is 1 or 2. Thus, for both of our sources, and especially for the secondary, the choice of α is not crucial. Consistent with this, we explicitly show that both DUSTY-2000 and SETTL-2005 spectra imply very similar T_{eff} for this object, in spite of the difference in α between the two sets of models.

The fundamental distinction between the DUSTY, COND, and SETTL synthetic spectra lies in their treatment of photospheric dust. All three models treat grain formation self-consistently, through chemical equilibrium calculations, and thereby also account for the depletion of chemical species that become sequestered in grains (Allard et al. 2001). However, the DUSTY models assume that all of the grains that form remain suspended in the photosphere; thus, these models include dust opacity as well. Conversely, the COND models assume that all of the grains have gravitationally settled below the photosphere and therefore neglect grain opacity altogether. These two scenarios represent the two extremes of dust behavior expected in cool dwarfs, as photospheric grains first form and then, with decreasing temperature, gradually drain out of the atmosphere. Finally, the SETTL models attempt to capture the true behavior of grains more faithfully, by self-consistently including the settling process itself, in addition to dust opacity. Thus, at relatively warm T_{eff} , when grains have formed and remain predominantly suspended in the atmosphere, or at very cool T_{eff} , when grains have completely rained out of the photosphere, the SETTL spectra resemble DUSTY and COND, respectively; in the intervening temperature regime, when grains have partially settled, SETTL spectra are intermediate between these two extreme models. Note that for $T_{\text{eff}} \gtrsim 2500$ K, the chemical equilibrium calculations indicate that *no* dust forms at all, so DUSTY, SETTL, and COND models are all exactly the same at these higher T_{eff} .

The treatment of dust settling in the SETTL models is based on the 3D radiative hydrodynamic (RHD) simulations by Ludwig (2003) and Ludwig et al. (2006); a full description can be found in the latter two articles and in Allard et al. (2003a). In brief, the mixing of atmospheric material, including grains, by convective overshoot motions can be parameterized by $v_{\text{mix}}(z) \equiv F_{\text{mass,up}}(z)/\langle \rho(z) \rangle$. Here v_{mix} is the velocity of mixing motions at some atmospheric height z , $F_{\text{mass,up}}(z)$ is the upward-directed mass flux at that location, and $\langle \rho(z) \rangle$ is the average mass density there. Note that more mixing is equivalent to less settling. The RHD simulations show that v_{mix} declines exponentially with atmospheric height above the Schwarzschild (convective stability) boundary. To a good approximation, the length scale of this exponential decline is found to be $H_{\text{mix}}(z) \propto H_P(z)(g_0/g)^{1/2}$, where $H_P(z)$ is the pressure scale height at z and g is the surface gravity in cgs units, normalized to a gravity of $g_0 = 10^5$ cm s $^{-2}$ (i.e., $\log g_0 = 5$). Thus, the simulations indicate that, all else being equal, there is greater mixing (less settling) at lower gravities. In the M dwarf simulations by Ludwig (2003), the constant of proportionality in the above relationship is ~ 0.5 , i.e., $H_{\text{mix}}(z) \approx 0.5H_P(z)$ for $\log g = 5$.

⁶ Available online at <http://perso.ens-lyon.fr/france.allard/Papers/Allard03.pdf>.

We have used two sets of SETTL-2005 spectra based on this formulation. In the first, mixing is parameterized by $H_{\text{mix}}(z) = 0.5H_P(z)(g_0/g)^{1/2}$, with $\log g_0 = 5$. As described above, this is the result directly implied by the RHD simulations. In the second, $H_{\text{mix}}(z) = 0.25H_P(z)(g_0/g)^{1/2}$. That is, the mixing scale height adopted in the latter models for the convective overshoot is half that indicated by the RHD calculations, thereby simulating less mixing (*more* settling). We note that the SETTL-2005 models we have described and used here differ slightly, in the settling parameterization employed, from the SETTL-2002 ones on the Lyon group's Web site.⁷ The 2005 models were kindly supplied to us by D. Homeier and F. Allard (2006, private communication).

An alternate prescription for describing grain settling has been put forward by Ackerman & Marley (2001), who parameterize the process through a grain sedimentation efficiency factor, f_{sed} . For the sake of completeness, we have compared our observations to these synthetic spectra as well, kindly supplied to us by D. Saumon (2006, private communication).

Finally, we also compare the data to Lyon theoretical evolutionary tracks, based on both DUSTY and COND atmospheres (Chabrier et al. 2000; Baraffe et al. 2003). In these evolutionary models, the atmospheric opacity acts as a boundary condition on the interior calculations; thus, for a given mass, the temporal evolution of the *spectral and photometric properties* does depend on the flavor of atmosphere adopted (DUSTY or COND). However, the *cooling properties* of brown dwarfs (i.e., the temporal evolution of T_{eff} and L_{bol} , and thus of radius and surface gravity) are negligibly affected by the opacity: $T_{\text{eff}}(t) \propto \kappa_R^{-1/10}$ and $L_{\text{bol}}(t) \propto \kappa_R^{-1/3}$ (Burrows & Liebert 1993; Baraffe et al. 2002). Consequently, we distinguish between the evolutionary tracks based on COND and DUSTY when comparing to the observed photometry of our sources, but not when comparing to their L_{bol} or T_{eff} .

We note that the JHK_s photometry for 2M1207A and 2M1207B, as well as for AB Pic B, which we also analyze, has been obtained in the 2MASS system, while the Chabrier et al. (2000) and Baraffe et al. (2003) evolutionary models supply predicted JHK in the CIT system. We have therefore converted the 2MASS values for 2M1207A, a late-M type source, to CIT using the transformations given by Carpenter (2001). For the L-type sources 2M1207B and AB Pic B, we have converted from 2MASS to CIT using the transformations given by Stephens & Leggett (2004). The resulting shift from 2MASS to CIT is ~ 0.1 mag in J and < 0.05 mag in H and K for all three objects; for 2M1207B and AB Pic B, these shifts are at most comparable to, or much less than, the uncertainties in their photometry.

The transformations derived by Stephens & Leggett (2004) are dependent on spectral type. For the conversions above, we have therefore nominally assumed L7.5 for 2M1207B and L1 for AB Pic B, to be consistent with the \sim L5–L9.5 and \sim L 1^{+2}_{-1} types assigned to them by Chauvin et al. (2004) and Chauvin et al. (2005b), respectively. In reality, the transformations are quite flat in the L regime: varying the assigned type over the entire L range changes the corresponding 2MASS-to-CIT transformations by $\lesssim 0.05$ mag (see Fig. 6 of Stephens & Leggett 2004). This is much less than the photometric error bars for 2M1207B and AB Pic B, so the uncertainty in their spectral type does not affect our analysis. Of more concern is the fact that the Stephens & Leggett (2004) transformations are derived for higher gravity field L and T dwarfs. Our objects are much younger and lower gravity ones, with correspondingly somewhat different spectral shapes (as discussed later), and hence presumably not subject to exactly the same filter transformations as the field dwarfs. Thus, ideally we

should compare our data to evolutionary models with predicted photometry in the same filter system as the observations (2MASS), instead of employing the reverse and more uncertain operation of transforming our data to the models' filters (CIT). While time constraints prevented us from obtaining the entire suite of evolutionary models in 2MASS filters, we therefore checked for potential systematics by computing 2MASS and CIT photometry for low- and high-gravity synthetic spectra (the same COND and DUSTY spectra used by the evolutionary models for photometry predictions) sampling late-M to mid-T temperatures (\sim 2500–1000 K). We found that while gravity does make a small difference, it is negligible for our purposes: the shifts from 2MASS to CIT magnitudes for the low-gravity ($\log g = 4.0$) synthetic spectra are in the same direction as, and within 0.05–0.1 mag of, the shifts predicted by the Stephens & Leggett (2004) transformations for higher gravity ($\log g = 5$ –5.5) field objects in the same spectral type range. These variations are again smaller than the uncertainties in the photometry of 2M1207B and AB Pic B; consequently, we are justified in simply adopting the Stephens & Leggett (2004) transformations for the purposes of this paper.

For 2M1207AB, we also show ground-based photometry in L' (Johnson-Glass system) and HST photometry in the F090M and F160W filters. We do have Lyon tracks with predicted photometry in these filters, so no data transformations were required for these.

Lastly, we note that all magnitudes cited are relative to Vega.

6. RESULTS

6.1. Common Proper Motion and J-Band Photometry

Using three VLT astrometric observations from 2004 April to 2005 March, Chauvin et al. (2005a) found that 2M1207AB very likely comprises a bound comoving system. With an improved estimate of the distance and two additional HST observations in 2004 August and 2005 April, Song et al. (2006) have confirmed this result to 16σ . Our J -band image from 2005 March 26 provides an additional data point in this series. We find a separation of 769 ± 10 mas between 2M1207A and 2M1207B (including centroiding errors) and a position angle of B with respect to A of $125.6^\circ \pm 0.7^\circ$. These are completely consistent with the Song et al. (2006) values, from the combined VLT and HST data, of separation = 773.0 ± 1.4 mas and P.A. = $125.37^\circ \pm 0.03^\circ$.

Our relative photometry between 2M1207A and 2M1207B implies $\Delta J = 7.0 \pm 0.2$; with $J = 13.00 \pm 0.03$ from 2MASS for the primary, we have $J = 20.0 \pm 0.2$ for 2M1207B. For comparison, the Song et al. (2006) HST NICMOS photometry with the F110M filter (the closest approximation to J in their observations) implies $\Delta F110M = 7.17 \pm 0.15$ and $F110M = 20.61 \pm 0.15$ for 2M1207B. These results are consistent with ours: the F110M filter (passband \sim 1.0–1.2 μm) covers only the blueward side of the J band, while both the F110M and J magnitudes we cite are relative to the A-type star Vega, which is very blue across the J band; the result is a fainter F110M magnitude for both objects compared to J .

6.2. Spectral Types

6.2.1. Previous Results

Gizis (2002) assigned a spectral type of M8 to 2M1207A, based on a comparison of various atomic and molecular indices in its low-resolution optical spectrum to those of field M dwarfs. This procedure is not ideal, since the optical spectra of very young, low-gravity late-M types are known to diverge somewhat from those of higher gravity field dwarfs. Optical types for such young

⁷ See [ftp://ftp.ens-lyon.fr/pub/users/CRAL/fallard](http://ftp.ens-lyon.fr/pub/users/CRAL/fallard).

objects have therefore also been obtained by fitting templates composed of combined M-type giant and dwarf spectra (Luhman 1999; Luhman et al. 2003; White & Basri 2003). Nevertheless, the resulting error in the Gizis (2002) typing appears small: as he shows, the gravity-sensitive VO indices in 2M1207A's optical spectrum, while stronger than in field M dwarfs (as expected), are comparable to those in the very young brown dwarf GY 141, which Luhman et al. (1997) have assigned a type of M8.5 through dwarf+giant fitting. Similarly, Mohanty et al. (2005) report that the temperature-sensitive TiO bands in high-resolution optical spectra of 2M1207A are well matched by those in $M8 \pm 0.5$ young brown dwarfs, where the latter have again been typed previously through dwarf+giant fitting. A spectral type of $M8 \pm 0.5$ thus appears acceptable for 2M1207A.

The situation has been more uncertain for 2M1207B. In the discovery paper, Chauvin et al. (2004) showed that its $H - K$ and $K - L$ colors were comparable to, or redder than, those of the reddest late-L field dwarfs. Meanwhile, their spectrum for it in the H band alone, at low S/N, appeared similar to that of L5–L9.5 field dwarfs. The colors implied by the Song et al. (2006) *HST* NICMOS photometry, covering roughly I to H bands, appear consistent with this mid- to late-L classification.

6.2.2. New Infrared Spectra

Figure 5 shows our HK spectra of 2M1207A and 2M1207B compared to those of field M6–L8 dwarfs. For 2M1207A, we see that the general slope of the SED from H to K , the shape of the K -band spectrum, and the depth of the CO band head at $2.3 \mu\text{m}$ are all comparable to those in the M8 dwarf (note that the CO band heads at longer wavelengths are degraded by noise in 2M1207A). We emphasize that an exact determination of infrared spectral type is not our goal here; we are simply pointing out that the overall appearance of the HK spectrum of 2M1207A is reasonably similar to that of an M8 dwarf, consistent with the optical spectral type assigned earlier.

However, there are also notable departures from the dwarf spectra. The most striking of these is the strongly peaked H -band profile in 2M1207A, in sharp contrast to the more rounded profiles in all of the other dwarfs. Such a triangular H -band shape seems to be a distinguishing feature of young late-type objects; for instance, it has been noted earlier in very young and cool brown dwarf candidates in the Trapezium cluster (Lucas et al. 2001). As Kirkpatrick et al. (2006) point out, this effect is related to the decrease in H_2 collisionally induced absorption (CIA) opacity at low gravities (§ 7.1.1; see also Borysow et al. 1997). Another marker of low gravity in 2M1207A is the very weak Na I absorption at $2.2 \mu\text{m}$, compared to the stronger absorption in the higher gravity field dwarfs.

The spectrum of 2M1207B is even more arresting. The deep H_2O absorption troughs in the H band are commensurate with a mid to late L-type object, as suggested by Chauvin et al. (2004); so is the large H_2O opacity in the K band. However, despite the relatively low S/N ($3-10 \sigma$), a triangular H -band profile is clearly visible, as in the primary and unlike any of the M or L dwarfs, indicating low gravity. Furthermore, 2M1207B exhibits a strikingly different K -band morphology compared to the field L dwarfs. Its SED in K peaks at a significantly longer wavelength, and its K flux relative to H is much higher than in the field dwarfs. The $H - K$ color of 2M1207B is consequently far redder than in typical L dwarfs, explaining the results of the Chauvin et al. (2004) photometry. These K -band effects arise from a combination of increasing photospheric dust and changes in $\text{H}_2\text{-CIA}$ and H_2O opacity with decreasing gravity (§ 7.1.1). Notice that the CO band head at $2.3 \mu\text{m}$ also appears much stronger in 2M1207B than in

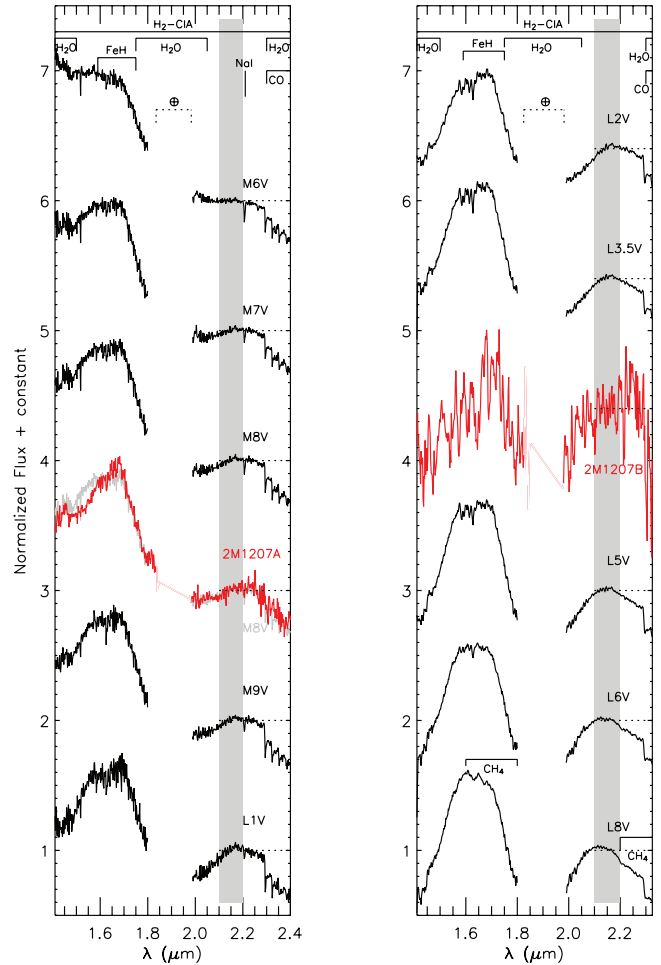


FIG. 5.—Comparison of our observed HK spectra of 2M1207A (red, left panel) and 2M1207B (red, right panel) with the spectra of field M and L dwarfs (black). All spectra have been normalized by their mean flux over $2.1-2.2 \mu\text{m}$ (region marked by gray strip) and offset for clarity (normalization levels shown by dotted lines). Opacity sources in various wavelength regions are marked: the $1.8-2.0 \mu\text{m}$ interval is dominated by telluric absorption and has been masked. The primary spectrum is overall similar to that of field M8–M9 dwarfs (M8 dwarf overplotted in gray for comparison) but shows a sharply peaked H -band profile and negligible Na I absorption, indicating low gravity. In the secondary, the overall strength of the H_2O absorption in H and K is similar to that in mid- to late-L dwarfs. However, the H -band profile is sharply peaked like in the primary, and the spectrum from H to K is much redder than in the field dwarfs, indicating low gravity and a dusty atmosphere. See § 6.2.2.

the L dwarfs (although we caution that poor S/N in this region of the secondary's spectrum may also be a contributing factor). In M types, deeper CO is associated with low gravity (e.g., Luhman & Rieke 1998); if this trend continues into the L class (as the atmospheric models suggest it does; § 7.1.1), it would be yet another signature of low gravity in 2M1207B.

In this context, it is worth noting that anomalously red IR spectra and deep CO have also been seen in the \sim L4.5 field object 2MASS 2224–0158 (Cushing et al. 2005); similarly red colors and a triangular H band identified in the \sim L0 source 2MASS 0141–4633 (Kirkpatrick et al. 2006); and anomalously red colors, a triangular H band, and deep CO seen in the L6.5 field dwarf 2MASS 2244+20 (McLean et al. 2003). Substantial photospheric dust and low gravity have been proposed to explain the first, low gravity to explain the second, and both effects may be at play in the third, in step with our conclusions here.

To summarize: while the general strength of H_2O opacity in its H and K bands indicates a mid- to late-L type for 2M1207B, the

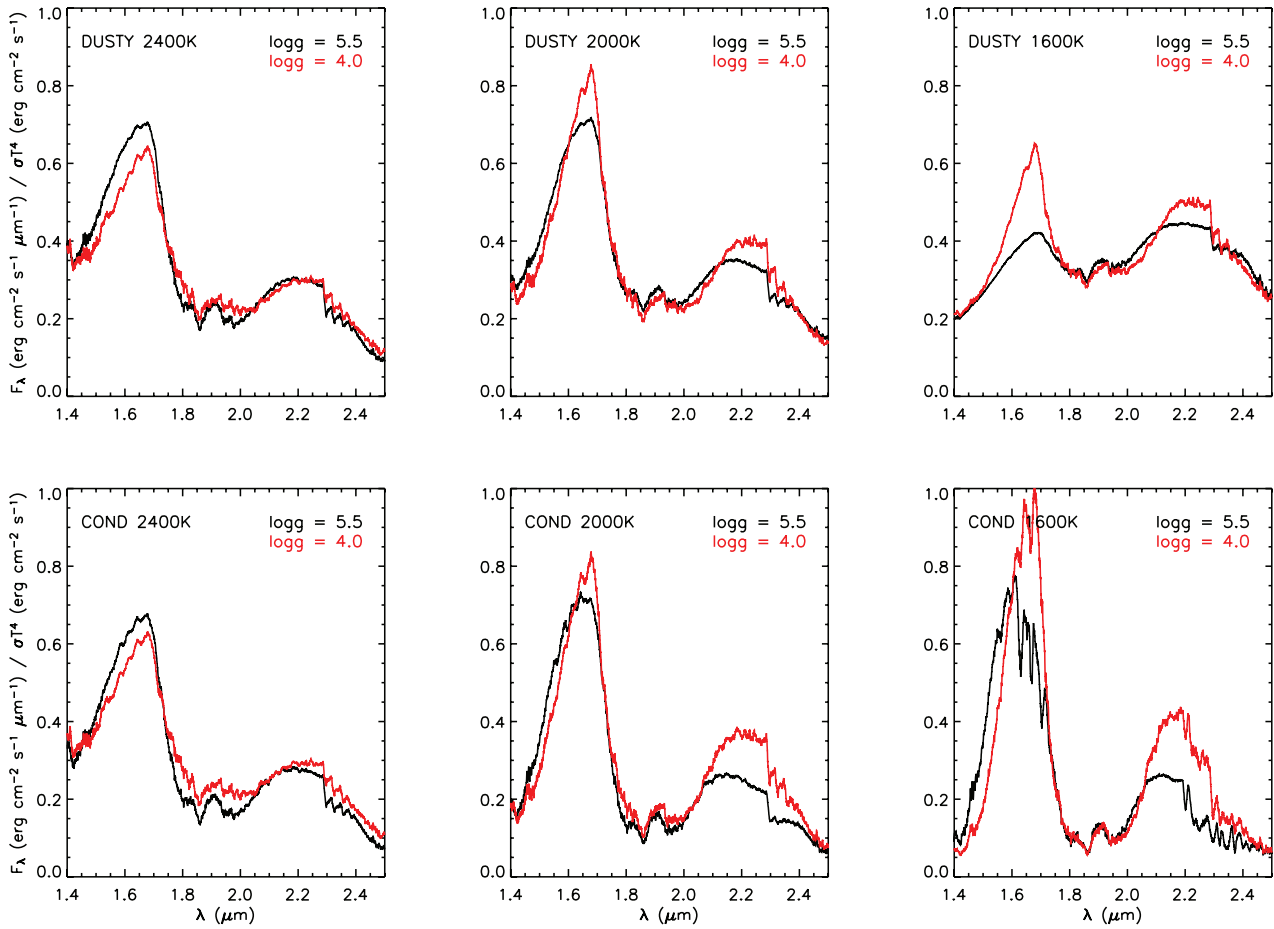


Fig. 6.—DUSTY and COND model fluxes (*top and bottom panels, respectively*), at different gravities ($\log g = 4.0$ in red and 5.5 in black) and T_{eff} (2400, 2000, and 1600 K; *left to right*). Spectra at every T_{eff} are normalized by the corresponding bolometric flux σT_{eff}^4 , to clearly illustrate relative differences due to various gravity, T_{eff} , and dust-related opacity effects. See § 7.1.1.

shape of its H band and the overall form of its SED from H to K depart strongly from typical L dwarf spectra. As such, it is impossible to assign a precise spectral type to 2M1207B based on HK comparisons to field L dwarfs. It is more fruitful to investigate the physical properties of 2M1207B (and 2M1207A) directly, through comparisons to synthetic spectra and evolutionary models.

7. ANALYSIS: EFFECTIVE TEMPERATURE AND MASS

7.1. Effective Temperature from HK Spectra

7.1.1. Trends in the Synthetic Spectra

To supply a physical basis for interpreting synthetic spectral fits to our data, we first discuss some salient trends in the model spectra with varying T_{eff} , gravity, and dust. Figure 6 shows DUSTY and COND models (described in § 5) for various T_{eff} (1600, 2000, and 2400 K) and two different gravities ($\log g = 4.0$ and 5.5). The following behaviors can be seen:

1. Dust starts to form in DUSTY and COND models only at $T_{\text{eff}} \lesssim 2500$ K. At higher temperatures, therefore, the two models are identical (not shown); at T_{eff} below but still close to 2500 K, they remain very similar since little dust has formed yet (e.g., 2400 K shown).

2. At a fixed gravity, DUSTY models become redder with decreasing T_{eff} : the combination of large dust opacity at shorter wavelengths and suppressed H_2O opacity at longer wavelengths in the presence of dust (back-warming by grains both dissociates H_2O

and creates a hotter, more transparent H_2O opacity profile) pushes the emergent flux redward. The effect is exacerbated at lower T_{eff} as more grains form and remain suspended in the photosphere. Conversely, COND models become bluer in the NIR with decreasing T_{eff} : without dust opacity (grains form but settle out), increasing H_2O and H_2 -CIA opacity at longer wavelengths forces emergent flux blueward, and the effect grows as the two opacities strengthen with falling T_{eff} (at sufficiently low T_{eff} , CH_4 absorption further magnifies this spectral blueing in the COND models). The crucial result, for our purposes, is that DUSTY models are always redder than COND ones in $H - K$, at a given T_{eff} and gravity.

3. In both COND and DUSTY spectra, lower gravity produces a more triangular H -band profile and shifts the peak in H and K redward. This can be understood as follows. On the one hand, the overall H_2O opacity in the H and K bands decreases with decreasing gravity, allowing more flux to emerge in these regions. Simultaneously, H_2 -CIA opacity (due to induced 1–0 quadrupolar moment of H_2), which peaks at $\sim 2.5 \mu m$ and declines at shorter wavelengths, also diminishes at lower gravities (Borysow et al. 1997). The combination of the two produces the observed changes in the H - and K -band shapes. For comparison, it is interesting to note that very large H_2 -CIA (higher than in normal field L dwarfs) is implicated in the flat and suppressed K band and blueward-slanted H band of metal-poor L dwarfs, such as 2MASS 0532+8246 (Burgasser et al. 2003b). These effects are opposite to those described here for low gravity/low H_2 -CIA. This is reasonable, since low metallicity produces higher pressures at a given

optical depth, while low gravity implies lower pressures, and it is fundamentally pressure that drives the behavior of H₂-CIA.

4. Finally, the 2.3 μm CO band head becomes deeper with lower gravity at a given T_{eff} , in both COND and DUSTY models. In the CO region, a major continuum opacity source is H₂O; at the lower pressures implied by lower gravity, the opacities of both molecules decrease. However, since H₂O is a triatomic molecule compared to the diatomic CO, its opacity decreases faster than that of CO. Consequently, the CO band heads appear deeper at lower gravity relative to the surrounding continuum.

7.1.2. Model Fits to HK Spectra: Procedure

We wish to determine T_{eff} for 2M1207A and 2M1207B from fits to synthetic spectra. As shown above, the shape of the spectrum is affected by temperature as well as gravity; to determine both *simultaneously* through spectral fitting requires analysis of spectral features at higher resolution and higher S/N than we possess. Instead, since it is temperature we are after, we *a priori* fix the gravity to the range implied by the evolutionary models for substellar objects at the age of 2M1207AB. This clearly makes our results dependent on the evolutionary models from the outset. However, since our subsequent mass estimates (as well as all analyses of this system by other researchers) are based on these models anyway, adopting them from the beginning is self-consistent, and not an additional drawback.

For ages of 5–10 Myr, the evolutionary models predict gravities of $\approx 4.0 \pm 0.25$ ($\log g$ in cgs) over the entire substellar domain. We therefore employ synthetic spectra with $\log g = 3.5$ –4.5 (step 0.25 dex) in our T_{eff} analysis. At each gravity, the observed HK spectra are compared to a range of model T_{eff} : 3000–2000 K DUSTY spectra for 2M1207A, and 2500–1500 K DUSTY spectra and 2500–900 K COND spectra for 2M1207B. The best-fit model spectrum is found via least-squares fitting to H and K simultaneously, as follows.

The model spectra are rebinned to the spectral resolution of the data ($R \sim 550$ and ~ 100 for 2M1207A and 2M1207B, respectively). Next, as a first guess for the appropriate normalization for comparing models and data, both are initially normalized by the mean of their respective fluxes over the range 2.1–2.2 μm , near the peak of the K band. However, while the current synthetic spectra are very sophisticated, they still contain significant opacity uncertainties (e.g., Allard et al. 2001; Leggett et al. 2001). Forcing concordance *a priori* between the models and data over a narrow wavelength range can thus lead to skewed results. Consequently, we allow the normalization of every model to vary from 0.5 to 2 times the initial guess, in steps of 1%, during the fitting process. This allows us to optimize the global fit of each model spectrum to the HK data. Our least-squares statistic is defined as

$$s^2 \equiv \frac{\sum_{i=1}^N [(nf_i^{\text{model}} - f_i^{\text{obs}})/f_i^{\text{obs}}]^2}{N},$$

where f_i^{model} and f_i^{obs} are the initially normalized model and observed fluxes in each wavelength bin i ; n is the varying normalization then applied to the model, ranging from 0.5 to 2 in steps of 0.01; and N is the total number of wavelength bins. Parameter s^2 therefore captures the average fractional deviation between the data and a model for a specified model normalization. For any given $T_{\text{eff}}/\log g$ model, the optimum fit to the data is obtained by finding the normalization n that minimizes s^2 . We note that the optimum n generally differs from our initial guess by <20%. The overall best-fit $T_{\text{eff}}/\log g$ model is then identified as the one with the minimum least-squares value s^2 among all of these normalization-optimized model spectra.

During the fitting, we mask regions of high telluric absorption (1.82–1.98 μm) and very low S/N (>2.5 μm for 2M1207A, >2.25 μm for 2M1207B, and <1.41 μm for both). Moreover, the model fits to 2M1207A are problematic over the range 1.5–1.7 μm , as discussed below; we have thus masked this region as well for the 2M1207A fits.

Finally, the validity of the best fit obtained, as well as the range of admissible T_{eff} values, is verified by examining all of the fits by eye.

7.1.3. Model Fits to HK Spectra: Results

Primary.—For 2M1207A, the left panel of Figure 7 shows the least-squares contours for normalization-optimized DUSTY models, with $T_{\text{eff}} = 2000$ –3000 K and $\log g = 3.5$ –4.5. The important quantity here is not the absolute but the relative value of the least squares, which signifies the relative merit of the fits; to portray this clearly, all of the least-squares values s^2 have been normalized (divided) by the global minimum in s^2 , obtained for the best-fit model. The best fit is nominally at $T_{\text{eff}} = 2650$ K, $\log g = 4.0$; however, we see that the fits are rather insensitive to gravity, and $T_{\text{eff}} \approx 2650$ K is the best match from $\log g = 3.5$ to 4.5. Changing the temperature by ± 200 K from this value worsens the fit significantly.

These conclusions are verified by examining the fits by eye. Figure 8 shows the model comparisons to the data at 2650 ± 200 K and $\log g = 3.5, 4.0$, and 4.5. At the best-fit T_{eff} of 2650 K, the models match the K -band flux, the redward side of the H band, and the H₂O absorption feature at $\leq 1.5 \mu\text{m}$ rather well at these gravities. The 2450 K models overestimate the H₂O opacity at $\leq 1.5 \mu\text{m}$ and begin to deviate from the observed shape of the K band, while the 2850 K models underestimate the H₂O opacity as well as the K -band flux. From these fits, we would be justified in adopting $T_{\text{eff}} \approx 2650 \pm 200$ K.

However, notice that all of the models overestimate the 1.5–1.7 μm flux, near the peak of the H band (as noted above, this region is excluded in the least-squares fitting). The $T_{\text{eff}} = 2650$ K, $\log g = 3.5$ model comes closest but is still not an adequate match. Such overprediction of H -band emission by the model spectra has been pointed out before, in comparisons to both field and young M types (e.g., Leggett et al. 2001; Lucas et al. 2001), and is ascribed to known inadequacies and incompleteness in the current H₂O line lists in the models at these relatively hot temperatures (Allard et al. 2001). Moreover, a forest of FeH lines dominating the ~ 1.58 –1.75 μm region in field M and L dwarfs has recently been identified (Wallace & Hinkle 2001; Cushing et al. 2003). These lines (thought to arise from the 0–0 band of the $E^4\Pi-A^4\Pi$ system) are not included in the current generation of synthetic spectra at all and would also tend to depress the model flux precisely where it is anomalously high now.

Given these H₂O and FeH opacity uncertainties in the infrared, one would ideally like to verify our HK-based T_{eff} with a more reliable diagnostic. TiO band heads in the optical provide just such a tool. Allard et al. (2000) showed that the new AMES-TiO line lists in the synthetic spectra provide a much better fit to the optical SEDs and photometry of M dwarfs. Mohanty et al. (2004a) subsequently demonstrated that the models match quite well the observed TiO band heads at $\sim 8400 \text{ \AA}$, in *high-resolution* spectra of very young mid- to late-M sources. Moreover, they found that this TiO band (specifically, triple-headed band at 8432, 8442, and 8452 \AA , identified as the $E^3\Pi-X^3\Delta$ system by Solf 1978) is highly temperature sensitive and simultaneously relatively gravity *insensitive*, ideal for fixing T_{eff} .

We have previously obtained high-resolution optical spectra of 2M1207A on Magellan (Mohanty et al. 2003). Following

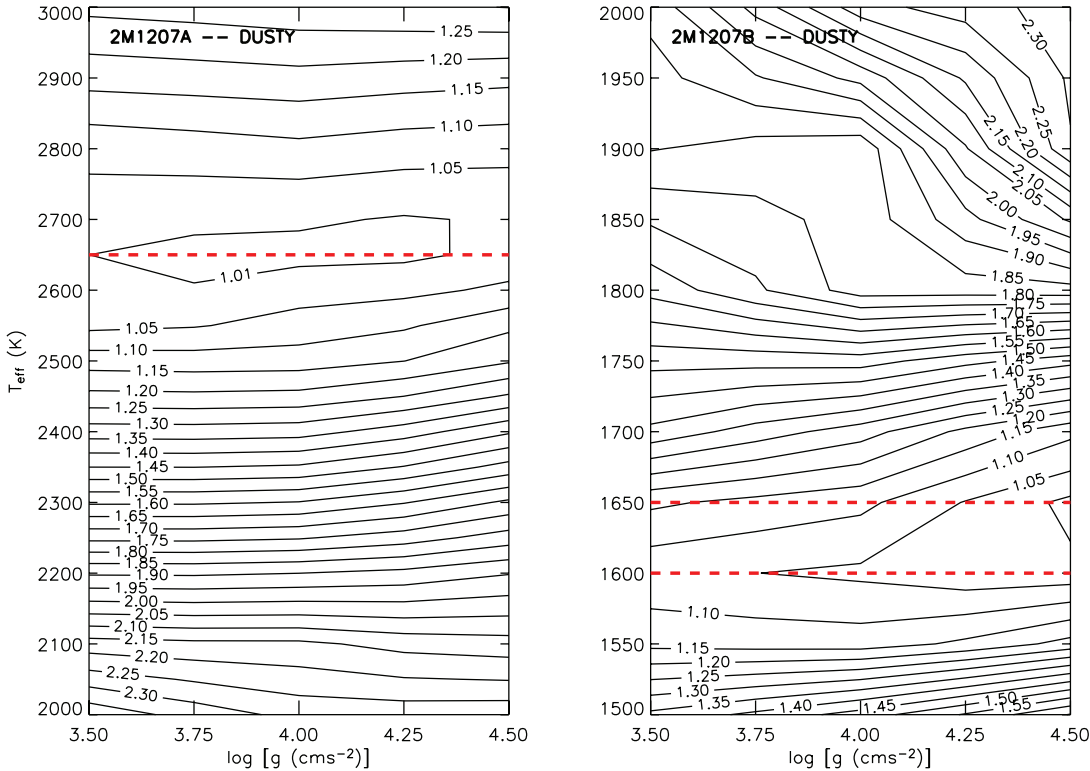


FIG. 7.—Contour plots of least-squares values (s^2) for DUSTY model fits to 2M1207A and 2M1207B. *Left:* Contours for 2M1207A. All s^2 are normalized by the minimum (best fit) value, obtained at $(T_{\text{eff}}, \log g) = (2600 \text{ K}, 4.0)$, to show relative merit of the fits. The fits are relatively insensitive to gravity, with best-fit $T_{\text{eff}} \approx 2600 \text{ K}$ over $\log g = 3.5\text{--}4.5$ (red dashed line). Note that the merit of the fits changes relatively slowly for $T_{\text{eff}} \gtrsim 2700 \text{ K}$ (contours are widely spaced) compared to below 2700 K (i.e., upper T_{eff} limit not as well constrained as lower). *Right:* Contours for 2M1207B. All s^2 are normalized by the minimum (best fit) value, obtained at $(T_{\text{eff}}, \log g) = (1650 \text{ K}, 4.5)$. The fits are again relatively insensitive to gravity, with best-fit $T_{\text{eff}} \approx 1600 \text{ K}$ over $\log g = 3.5\text{--}4.0$ and 1650 K at $\log g = 4.5$ (red dashed lines). See § 7.1.3.

Mohanty et al. (2004a), therefore, we derive T_{eff} by comparing its TiO band heads to synthetic spectra. The results are plotted in Figure 9. The best-fit model, at 2500 K, clearly matches the data remarkably well: both in the TiO band heads (except a small mismatch to the very core of the $\lambda 8432$ band head⁸) and in the surrounding continuum. Changing T_{eff} by only ± 50 K produces small but noticeable departures from the data, in the $\lambda\lambda 8442$, 8452 band strengths as well as in the average continuum flux redward of 8452 Å, while ± 100 K changes yield clearly worse fits.

From the TiO data alone, therefore, we would infer $T_{\text{eff}} = 2500 \pm 100$ K for 2M1207A. Crucially, this is within 150 K of the 2650 K derived from the *HK* low-resolution data and well within the combined errors of the optical and infrared fits (100–200 K in each). This confirms the general validity of the *HK* fits (at the ~ 200 K precision we desire in this work) despite the remaining uncertainties in the model H₂O and FeH opacities.

From the above analyses, the most conservative estimate of 2M1207A's temperature would be $T_{\text{eff}} = 2400\text{--}2850$ K, the union of the full ranges implied by the optical and NIR fits. The lower limit, compatible with both the TiO and *HK* data, is accept-

able. However, the upper limit, which comes from the *HK* fits alone, appears too high: on the one hand, the *HK* fits become less sensitive to T_{eff} above ~ 2700 K (as shown by the contours in the left panel of Fig. 7, which become much more widely spaced at higher T_{eff} than at lower ones); on the other hand, the TiO fits, which do remain very sensitive to higher temperatures, appear incompatible with T_{eff} much higher than ~ 2600 K (as shown by the large mismatch between the models and TiO data at 2700 K, in Fig. 9). A safe but better estimate of the T_{eff} range is therefore $\sim 2400\text{--}2700$ K, which includes the best-fit T_{eff} implied by both the optical and NIR and the best limits compatible with both. Thus, we finally adopt $T_{\text{eff}} \approx 2550 \pm 150$ K for 2M1207A (where the mean is the middle of the range and also falls between the TiO and *HK* best fits). As we demonstrate below, this estimate is also in agreement with the NIR colors of 2M1207A ranging from J to L' (§ 7.4).

Secondary.—For 2M1207B, the right panel of Figure 7 shows the least-squares contours for normalization-optimized DUSTY and COND models with $T_{\text{eff}} = 1500\text{--}2000$ K and $\log g = 3.5\text{--}4.5$. Again, all of the least-squares values s^2 have been normalized by the global minimum in s^2 , obtained for the best-fit model. As in the primary, we see that the fits are rather insensitive to gravity over the range considered; the best fit to the DUSTY models is at $T_{\text{eff}} \approx 1600$ K from $\log g = 3.5$ to 4.0, rising to ~ 1650 K at $\log g = 4.5$. Changing the temperature by ± 100 K from this value worsens the DUSTY fits significantly. We note that all of the COND fits are far worse and not shown (but see below and Fig. 10).

These conclusions are verified by examining the fits by eye. Figure 10 shows the model comparisons to the data for

⁸ The 2500 K model is slightly deeper than the data in the core of the $\lambda 8432$ band head, which appears weakly gravity sensitive over the 1 dex range in $\log g$ plotted: while the fit to the core is best at $\log g < 4.5$ (consistent with the evolutionary model prediction of $\log g \sim 4.0$ for brown dwarfs at 5–10 Myr), a slight mismatch persists down to $\log g = 3.5$ (the lowest gravity we examine). The 2500 K model also does not completely reproduce the relatively weak absorption feature at 8440 Å, just blueward of the $\lambda 8442$ band head. However, such small deviations between the data and model spectra are to be expected, even for the best fits, considering the huge number of TiO line opacities involved in matching the data at high spectral resolution.

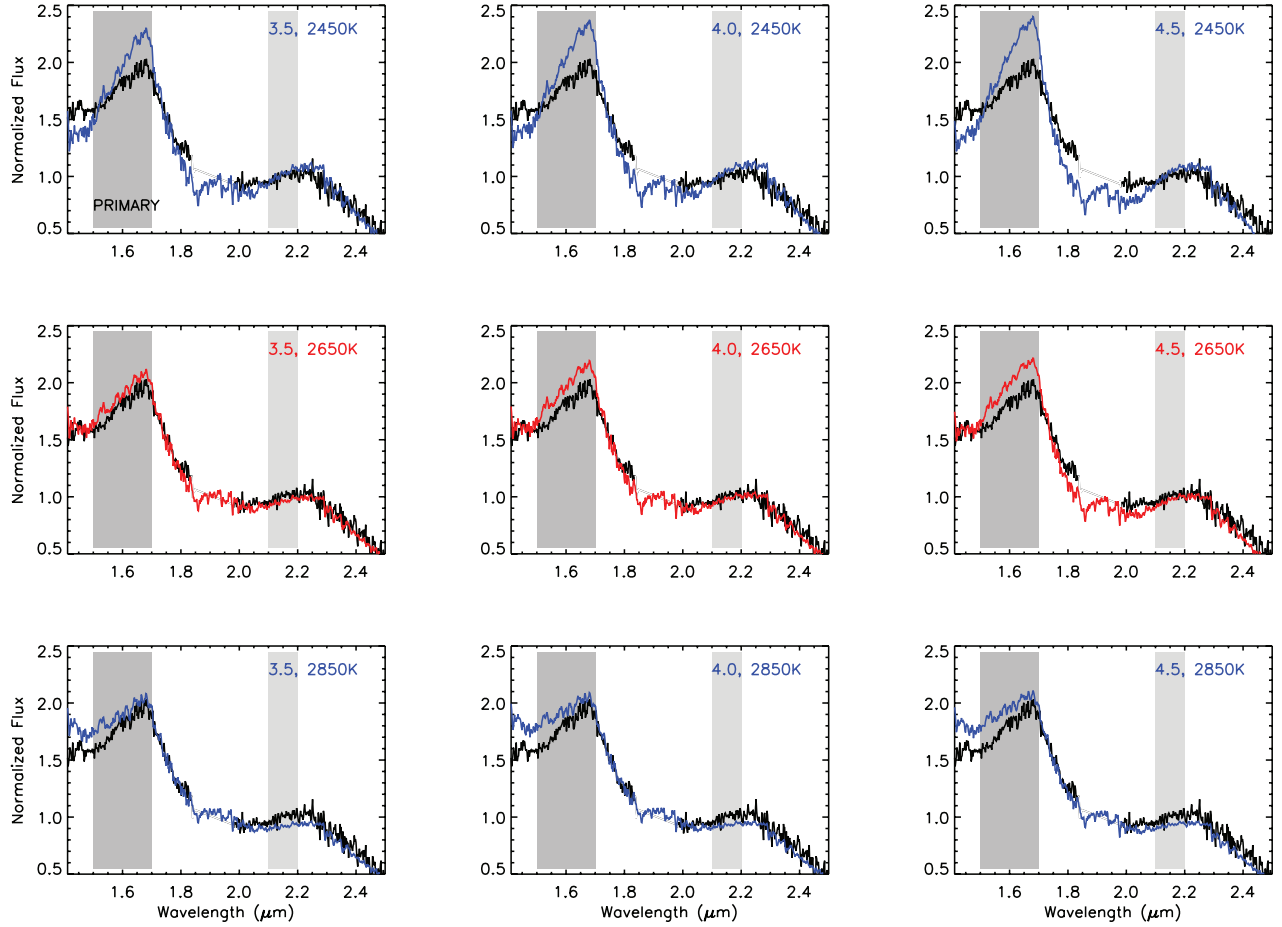


Fig. 8.—Observed *HK* spectrum of 2M1207A (black) compared to DUSTY models at various T_{eff} (increasing from top to bottom) over the expected range in gravities ($\log g = 3.5–4.5$, left to right). The dark gray strip on the left of each plot shows the region excluded during fitting ($1.5–1.7 \mu\text{m}$). The observed spectrum is normalized by its mean flux over $2.1–2.2 \mu\text{m}$ (region marked by the light gray strip on the right of each plot). Each model is shown at its optimum normalization, as described in § 7.1.2. Best-fit models (see contour plot in the left panel of Fig. 7), at 2650 K, are shown in red; the acceptable range in T_{eff} fits (2650 ± 200 K) is shown in blue. Note the overluminosity in the models over $1.5–1.7 \mu\text{m}$ compared to the data at all T_{eff} and $\log g$ shown, due to model H₂O and FeH opacity problems; this is why this region is excluded in the fits. See § 7.1.3.

$T_{\text{eff}} = 1500–1800$ K and $\log g = 3.5, 4.0$, and 4.5 . Despite the noise in the data, it is evident that the DUSTY 1600 K models reproduce the general shape of the *HK* spectrum very well at these gravities; the 1500 K DUSTY models are clearly redder, and the 1700 K models clearly bluer, than the data. Since DUSTY models become bluer with increasing temperature, T_{eff} significantly higher than 1700 K is inadmissible (as shown in Fig. 10 by the very poor match to 1800 K DUSTY). Similarly, since the 1500 K model is already too red and DUSTY spectra become redder with decreasing T_{eff} , temperatures significantly lower than 1500 K are not admissible either, in the context of DUSTY models. Conversely, the 1500 K COND model is far bluer than the data and also a poor match to the individual *H*- and *K*-band profiles; since these models become even bluer with lower temperature, $T_{\text{eff}} < 1500$ K yields even poorer COND fits (not shown).

In Figure 11 we further compare our data for 2M1207B to two flavors of SETTL models (differing by a factor of 2 in the assumed convective mixing efficiency in the overshoot layers; see § 5), over a range of T_{eff} at $\log g = 4.0$. In both cases, we see that models with $T_{\text{eff}} \approx 1500–1700$ K provide acceptable fits to the data, while cooler ones deviate sharply. In particular, the strong CH₄ absorption that depresses the flux at $\geq 2.2 \mu\text{m}$ in the synthetic spectra for $T_{\text{eff}} < 1500$ K is notably absent in 2M1207B. We also note that the more efficient mixing (less settling) model matches

the spectral shape slightly better, consistent with our earlier finding that DUSTY (no settling) spectra provide good fits to the data at the same T_{eff} . Very similar results are obtained on comparing our data to the f_{sed} models (kindly provided to us by D. Saumon; not plotted): $T_{\text{eff}} < 1500$ K is not compatible with the data, and good fits are obtained with significantly less sedimentation ($f_{\text{sed}} = 2$) than required for field L and T dwarfs ($f_{\text{sed}} \sim 3–5$; Marley et al. 2002, Knapp et al. 2004).

Putting all of this together, we conclude that $T_{\text{eff}} \approx 1600 \pm 100$ K is appropriate for 2M1207B and that 1500 K is a lower bound on plausible T_{eff} for this object regardless of which spectral models are used. Moreover, the model comparisons strongly indicate a dusty atmosphere with little grain sedimentation. The diminished degree of settling, compared to field L dwarfs at similar T_{eff} , is not very surprising, since the surface gravity of 2M1207B (based on the evolutionary models for its age) is lower by at least an order of magnitude. Henceforth, therefore, we refer only to the full DUSTY models.

As an aside, we note that the ~ 1600 K DUSTY and SETTL models that best fit 2M1207B's *HK* spectrum are able to fit the peak of the *H* band adequately: there is no obvious sign that the synthetic spectra at these temperatures overestimate the flux over $1.5–1.7 \mu\text{m}$, unlike in the case of 2M1207A at higher T_{eff} . Consequently, we have not masked out this region during our model

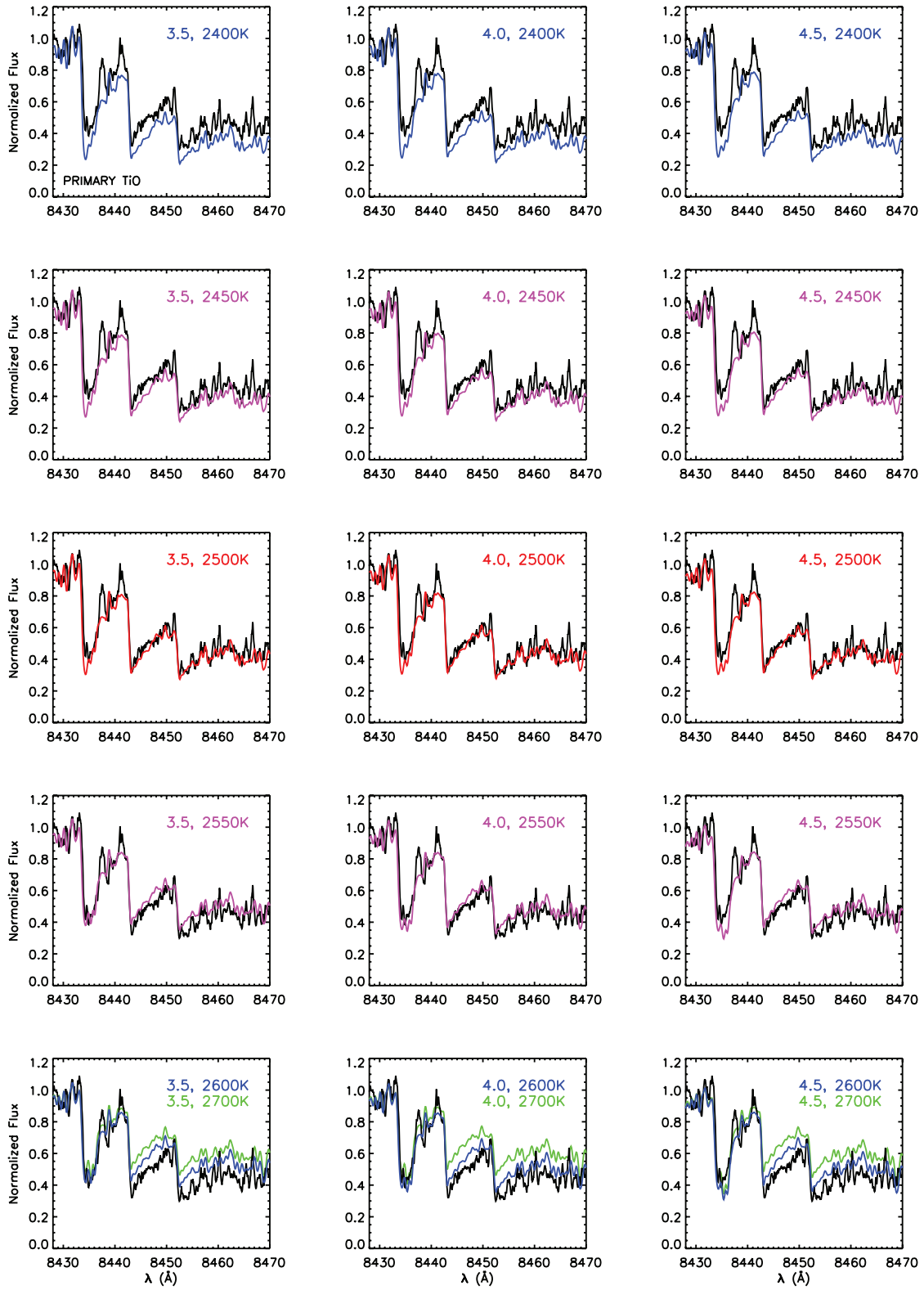


FIG. 9.—Observed TiO triple-headed band in high-resolution optical spectrum of 2M1207A (black), compared to DUSTY models at various T_{eff} (increasing from top to bottom) over the expected range in gravities ($\log g = 3.5\text{--}4.5$, left to right). Best-fit models, at 2500 K, are shown in red; models offset from this by ± 50 K are shown in magenta; models offset by ± 100 K are shown in blue. The TiO bands are highly insensitive to gravity but extremely sensitive to T_{eff} : offsets of ± 50 K from the best fit produce a small but discernible worsening in the fit, and offsets of ± 100 K are clearly worse. Note that the 2700 K models (green, bottom row) are completely inconsistent with the TiO data. See § 7.1.3.

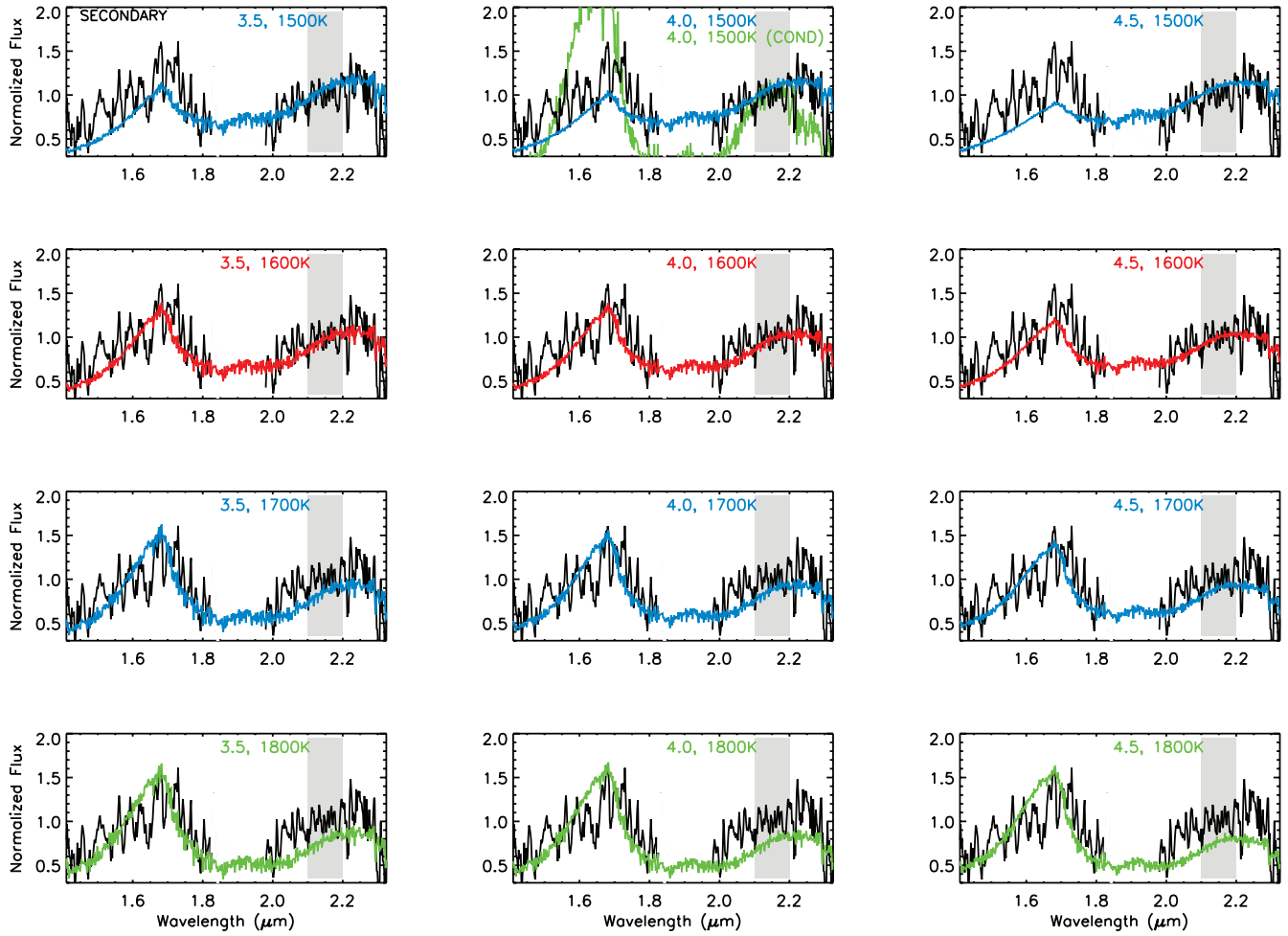


FIG. 10.—Observed *HK* spectrum of 2M1207A (black) compared to DUSTY models at various T_{eff} (*increasing from top to bottom*) over the expected range in gravities ($\log g = 3.5\text{--}4.5$, left to right). Data and models are normalized in the same fashion as in Fig. 8. Best-fit models (see contour plot in the right panel of Fig. 7), at 1600 K, are shown in red; the acceptable range in T_{eff} fits (1600 ± 100 K) is shown in blue; models at 1800 K are shown in green for comparison. The best-fit models reproduce the data well, within the uncertainties of the noise. The DUSTY fit is clearly very poor by 1800 K. A COND model at 1500 K and $\log g = 4.0$ (green, top middle panel) is also shown for comparison and is a very poor fit to the data: it is much bluer than 2M1207B and also shows strong CH₄ absorption at $\geq 2.2\mu\text{m}$, which is entirely absent in the data. See § 7.1.3.

fitting to 2M1207B (but see below). This lack of any obvious problem in the secondary, compared to the primary, is possibly connected to the behavior of FeH opacities: in field dwarfs, FeH bands are very strong in the *z*-, *J*-, and *H*-band spectra of late M dwarfs but weaken considerably by mid to late L (Burgasser et al. 2002; Cushing et al. 2003). If this trend holds for young M and L dwarfs as well, it could explain our result: since the *H*-band FeH opacities are not yet incorporated in the current synthetic spectra, a mismatch would be seen for the late-M primary where these opacities are important, but not in the mid- to late-L secondary where the FeH absorption is much weaker.

On the other hand, one might postulate that a problem with the predicted flux at the *H*-band peak does persist for the secondary as well. That is, perhaps the good fit we obtain at ~ 1600 K is coincidental; instead, a different T_{eff} model, which we have ruled out due to overluminosity in the *H* band, is actually the appropriate one. We do not think this is plausible, for two reasons. First, test fits to the secondary with the $1.5\text{--}1.7\mu\text{m}$ region masked out (not shown) yield the best match to the data at very similar T_{eff} ($1650\text{--}1700$ K). Second, as shown below, the 1600 K models also well reproduce all of the colors of the secondary from $\sim I$ to L' (§ 7.4). Nevertheless, we emphasize that if our T_{eff} for 2M1207B from *HK* fitting is skewed by a spurious model over-

luminosity in the *H*-band peak, then the true T_{eff} of the secondary must be *higher* than we estimate, not lower. As the DUSTY fits in Figure 10 show, the 1500 K DUSTY models, while giving an adequate fit to the data in *K*, are already *fainter* than the data in *H* rather than brighter. Going to lower T_{eff} only exacerbates this effect since DUSTY models become redder with decreasing temperature. At higher T_{eff} , on the other hand, the trend is reversed as the DUSTY models become bluer (e.g., see 1800 K model in Fig. 10); normalizing them to match the data in *K* would indeed make them overluminous in *H*. If this is due to model opacity problems in *H*, then T_{eff} may be higher than our estimate (although not much higher: for $T_{\text{eff}} \gtrsim 1900$ K, not shown, the DUSTY models also deviate from the observed H₂O absorption at $\leq 1.5\mu\text{m}$). A similar conclusion also holds for the SETTL fits. While T_{eff} may be somewhat higher than our estimate from the *HK* fits, if model problems exist in the *H* band, T_{eff} lower than ~ 1500 K is ruled out: regardless of model opacities in the *H* band, the data do not show the strong *K*-band CH₄ absorption that appears in the SETTL models at < 1500 K. We conclude that, at the least, the *HK* spectral synthesis sets a strong lower limit of ~ 1500 K on the effective temperature of 2M1207B.

Finally, we point out that the temperatures we have inferred for 2M1207A and 2M1207B, 2550 ± 150 K and 1600 ± 100 K,

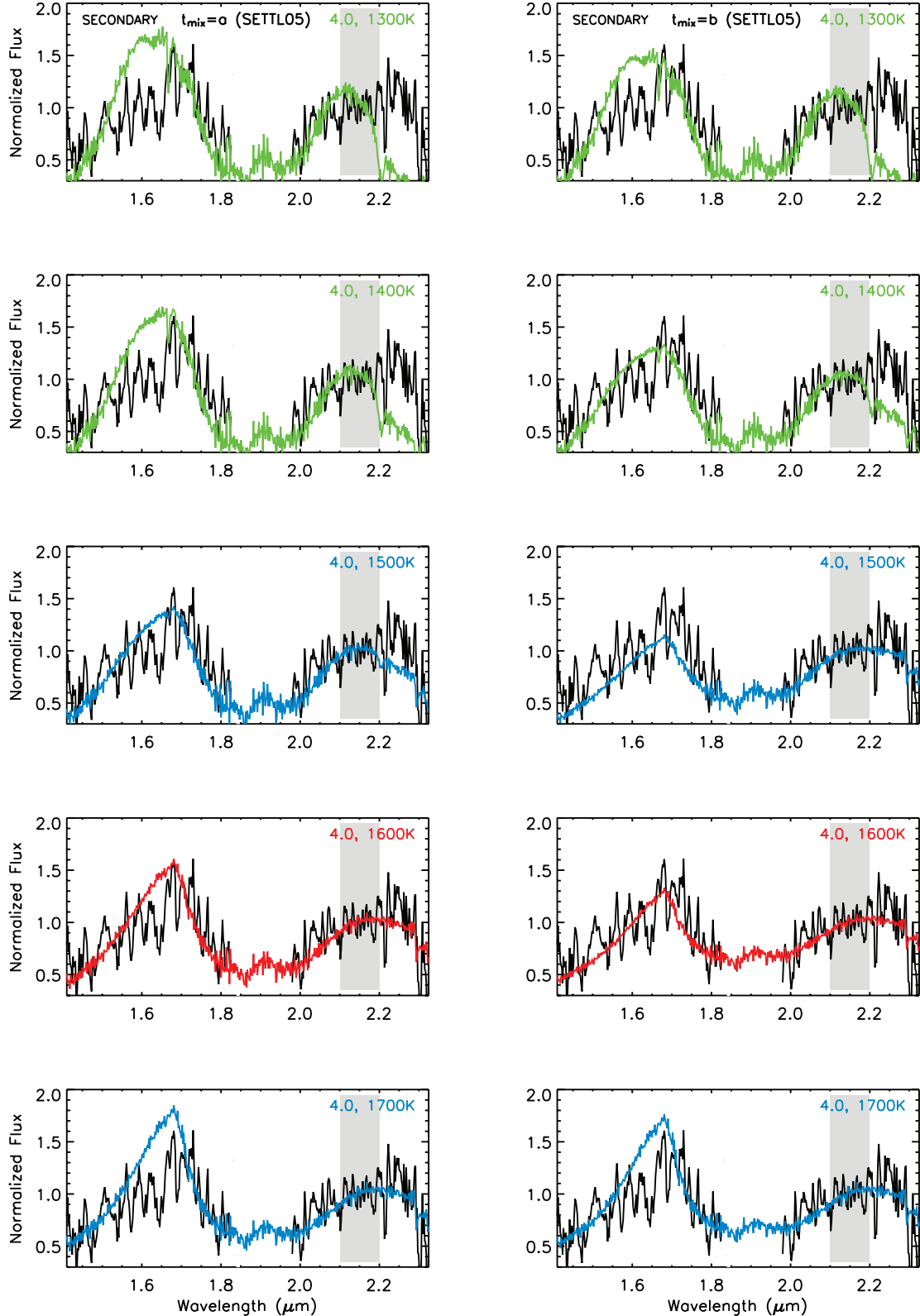


FIG. 11.—Observed *HK* spectrum of 2M1207B (black) compared to SETTL models at various T_{eff} (increasing from top to bottom), at the representative gravity of $\log g = 4.0$. Data and models are normalized in the same fashion as in Fig. 8. Left panels show SETTL models with less efficient mixing (more settling), compared to the models on the right (see model description in § 5). For both sets of models, the best-fit T_{eff} , 1600 K, is shown in red; the range in T_{eff} fits bracketing the data (1600 ± 100 K) is shown in blue; models with $T_{\text{eff}} < 1500$ K (1400 and 1300 K) are shown in green. The best-fit SETTL models reproduce the data quite well, similar to the best-fit DUSTY models in Fig. 10; the “less settling” model, on the right, appears to be a slightly better match to the observed *H*-band profile. Models at < 1500 K are very poor fits to the data; at these T_{eff} , much of the dust has settled out of the atmosphere in these models, bringing them closer to COND: they are much bluer than the observed spectrum, with strong CH₄ absorption at $\geq 2.2 \mu\text{m}$ that is not evident in the data. See § 7.1.3.

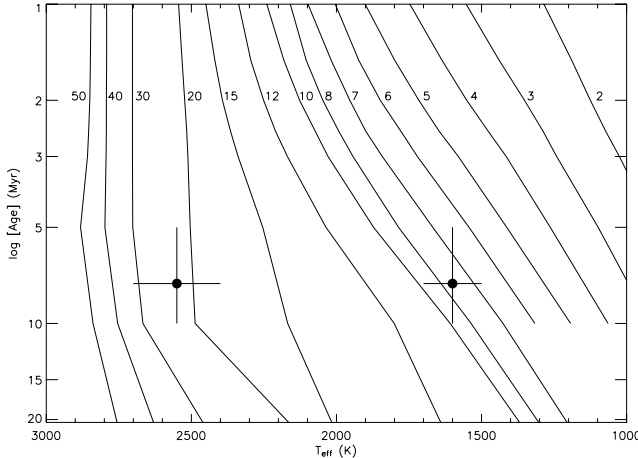


FIG. 12.—Comparison of 2M1207A and 2M1207B to the Lyon theoretical evolutionary tracks, in the age- T_{eff} plane. For our adopted age (5–10 Myr) and spectroscopically derived T_{eff} for the two components (primary: 2550 ± 150 K; secondary: 1600 ± 100 K), the tracks imply masses of ~ 18 – $30 M_{\text{Jup}}$ and 6 – $10 M_{\text{Jup}}$ for 2M1207A and 2M1207B, respectively. See § 7.2.

respectively, are fully consistent with their approximate spectral types (late M and mid to late L), at least when compared to field dwarfs of similar type with empirically determined T_{eff} (Golimowski et al. 2004). This is discussed further in § 8.3.

7.2. Mass from Age- T_{eff}

In Figure 12 we plot the latest Lyon theoretical models (Chabrier et al. 2000) for the temporal evolution of substellar temperatures. The isochronal age of TWA is $\sim 8^{+4}_{-3}$ Myr (Song et al. 2003; Zuckerman & Song 2004; Chauvin et al. 2004). Combining this with our derived T_{eff} for 2M1207A and 2M1207B and comparing to the Lyon evolutionary predictions yields $M_A \approx 18$ – $30 M_{\text{Jup}}$ and $M_B \approx 6$ – $10 M_{\text{Jup}}$. We recall from § 5 that the time evolution of global properties such as T_{eff} in the evolutionary models is insensitive to the particular atmospheres used (COND or DUSTY). Accordingly, our mass estimates (once T_{eff} is determined) are also nearly independent of the choice of atmosphere in the Lyon evolutionary models.

On the other hand, there are certainly differences between the evolutionary models constructed by different groups, due to varying assumptions about initial conditions and interior physics. In particular, for ages of 5–10 Myr, models by the Tucson group (Burrows et al. 1997) predict that masses $\lesssim 10 M_{\text{Jup}}$ are 5%–10% (100–150 K) cooler and 20%–30% fainter than in the Lyon models. Conversely, masses of ~ 15 – $50 M_{\text{Jup}}$ are 5%–10% hotter and 20%–40% brighter in the Tucson models than in the Lyon ones (for more on Lyon/Tucson differences see Burgasser 2004). Consequently, given our derived T_{eff} and adopted age for 2M1207AB, the Tucson tracks imply a mass for 2M1207A lower than our Lyon estimate by $\sim 3 M_{\text{Jup}}$ and a mass for 2M1207B higher than our Lyon estimate by $\sim 1 M_{\text{Jup}}$, systematic but small shifts compared to the mass uncertainties arising from T_{eff} and age error bars.⁹

Our Lyon mass for the primary, $M_A \approx 24 \pm 6 M_{\text{Jup}}$, is in good agreement with that inferred earlier by Gizis (2002) and Mamajek (2005). However, our secondary mass, $M_B \approx 8 \pm 2 M_{\text{Jup}}$, is significantly higher than asserted in previous studies ($\sim 5 M_{\text{Jup}}$, Chauvin et al. 2004; Song et al. 2006; 3 – $4 M_{\text{Jup}}$, Mamajek 2005).

⁹ The numbers given here for the Tucson tracks are calculated with the Web-based calculator, based on Burrows et al. (1997), supplied by the Tucson group at <http://zenith.as.arizona.edu/~burrows/>.

This is the key point of our work, and it is *not* affected by the choice of Lyon versus Tucson tracks. The previous estimates cited here were also based on the Lyon models, like ours; employing Tucson tracks instead shifts all of the inferred masses systematically, while leaving unchanged the *relative* differences between our mass estimates and previous ones. We return in §§ 7.4, 7.5, and 8 to the reasons for this discrepancy in the mass of 2M1207B. For now, we proceed to obtain a second set of mass estimates from color-color comparisons.

7.3. Mass from Colors

Figure 13 shows Lyon theoretical isochrones for substellar masses, at two ages (5 and 10 Myr) bracketing the expected range for TWA and in two color-color planes: $J - H$ versus $H - K$ and $H - K$ versus $K - L'$. Isochrones are shown for both COND and DUSTY cases (as mentioned in § 5, the particular atmosphere adopted as outer boundary condition in the evolutionary models does matter when examining the emergent SED). Notice that for masses $\gtrsim 30 M_{\text{Jup}}$, the COND and DUSTY isochrones become identical because at the T_{eff} corresponding to these masses at 5–10 Myr, no photospheric dust has formed yet. At smaller masses (i.e., lower T_{eff}), burgeoning grain formation causes the COND and DUSTY isochrones to diverge, with DUSTY models becoming substantially redder in all of the infrared colors. Comparing these to the observed colors of 2M1207A and 2M1207B, we find the following:

1. *Primary*.—2M1207A lands perfectly on the 5–10 Myr isochrones in the $[H - K]$ – $[K - L']$ plane. The implied mass is 20 – $30 M_{\text{Jup}}$, in complete agreement with the value derived above from age- T_{eff} considerations. While COND and DUSTY are almost indistinguishable at these masses, close examination reveals a slightly better match to DUSTY, as expected when grains first start to appear. On the other hand, the primary is somewhat offset from the isochrones in the $[J - H]$ – $[H - K]$ plane. The absence of such an effect in $[H - K]$ – $[K - L']$ suggests a discrepancy with the model $J - H$ alone. Indeed, shifting the Lyon isochrones to redder $J - H$ by 0.2 mag produces a good match to the primary, again at 20 – $30 M_{\text{Jup}}$. A ~ 0.2 mag offset is also seen in $J - K$, in a $[J - K]$ – $[H - K]$ plot (not shown). In fact, an analogous $J - K$ offset is known to exist between the Lyon models and field M dwarfs, with the former again being too blue by 0.2 mag (Allard et al. 2000, 2001). As the latter authors discuss, this may be due to remaining incompleteness, at relatively warm temperatures, in the AMES-H₂O line lists used in the synthetic spectra (FeH opacities may also play a role; see § 7.4). Given the qualitative and quantitative correspondence between our and the field M dwarf results, we are justified in applying a +0.2 mag correction to the Lyon isochrones in $J - H$ (or, equivalently, in $J - K$) for this source. The final outcome is that the same mass of 20 – $30 M_{\text{Jup}}$ is implied for 2M1207A from both color-color diagrams and the age- T_{eff} comparisons.

2. *Secondary*.—The observed colors of 2M1207B are in very good agreement, within the errors, with the 5–10 Myr DUSTY isochrones in both $[J - H]$ – $[H - K]$ and $[H - K]$ – $[K - L']$ planes. The implied mass is ~ 6 – $11 M_{\text{Jup}}$, identical to that derived from the age- T_{eff} model comparisons. Notice that the secondary lies very far from the COND isochrones in these color-color plots, bolstering our earlier conclusion that grains remain suspended in its atmosphere.

7.4. Effective Temperature from Colors

The agreement in mass between the color-color and age- T_{eff} techniques fundamentally means that the synthetic spectra that

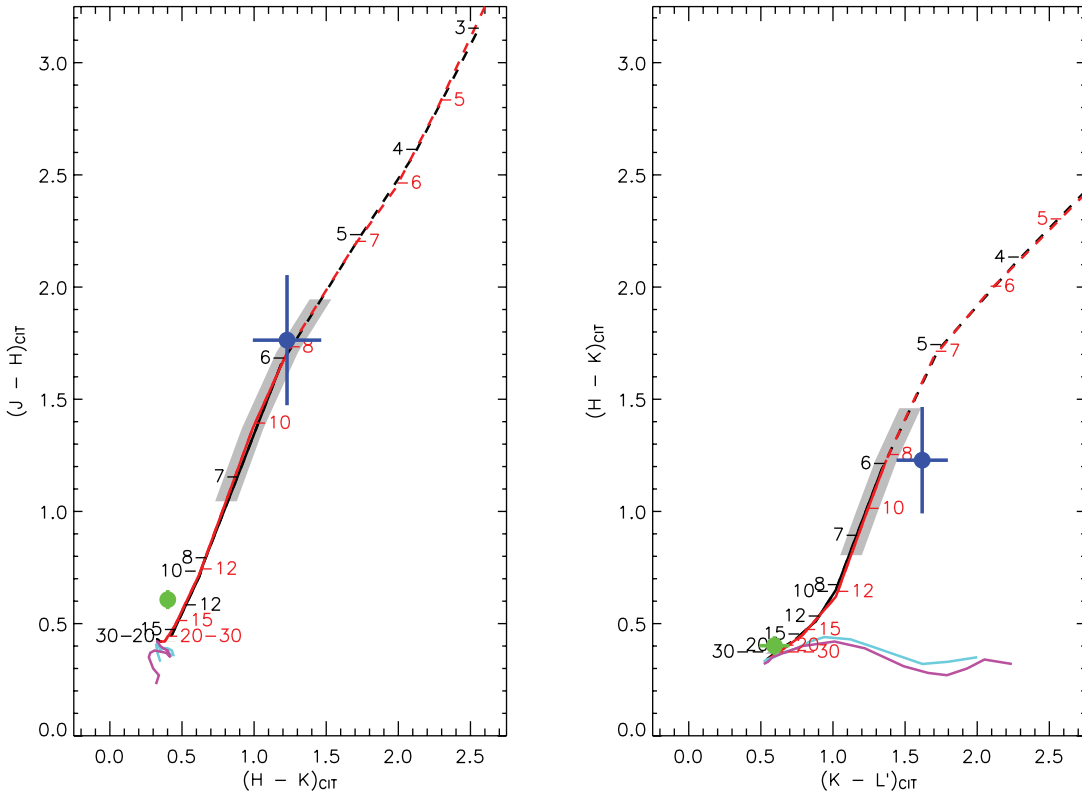


FIG. 13.—Comparison of 2M1207A and 2M1207B to Lyon theoretical color-color diagrams. All observed JHK are converted to the CIT system (see § 5). DUSTY isochrones at 5 and 10 Myr are shown in black and red, respectively, with the corresponding masses marked; COND isochrones at 5 and 10 Myr for the same range in masses are shown in aqua and magenta, respectively. Green filled circles represent the observed colors of 2M1207A, and blue filled circles denote 2M1207B; 1σ error bars in photometry are shown for both. The gray filled zones indicate the range in model colors corresponding to our spectroscopically derived range in T_{eff} (1600 ± 100 K) for 2M1207B. Left: $J - H$ vs. $H - K$. Right: $H - K$ vs. $K - L'$. See § 7.3.

best fit the observed HK spectra at a particular T_{eff} also faithfully reproduce the shape of the SED (i.e., colors) all the way from J to L' .

This is explicitly illustrated in the top left and top middle panels of Figure 14. We earlier derived spectroscopic $T_{\text{eff}} = 2550 \pm 150$ K and 1600 ± 100 K for 2M1207A and 2M1207B, respectively. The plots show the DUSTY colors for these T_{eff} (at $\log g \approx 4.0$, as deemed appropriate by the Lyon tracks), compared to the data for the primary and secondary. Not surprisingly (since the T_{eff} were determined from spectral fits in the HK region), the synthetic colors match the observed $H - K$ for both objects. In addition, as expected, the models fit reasonably well the $J - H$ and $K - L'$ colors in both, especially after correcting for the known systematic offset of 0.2 mag in the model $J - H$ described earlier. We note that for 2M1207B, the $JHKL'$ colors are best matched by 1550 ± 50 K, slightly lower than the mean, but within the 1600 ± 100 K range from our HK spectral fits.

For both objects, we also plot in the top left and top middle panels of Figure 14 the HST [F090M – F160W] colors observed by Song et al. (2006), corresponding roughly to $I - H$. For 2M1207A, we see that the DUSTY model at the spectroscopic $T_{\text{eff}} \sim 2550$ K appears too blue, by ~ 0.3 – 0.4 mag, compared to the HST data. The [F090M – F160W] color is best matched instead at 2250 K, cooler than the 2550 ± 150 K models that fit both the HK spectra and the $JHKL'$ colors. An analogous offset of ~ 0.3 mag, in $I - K$, is also seen for field mid-M dwarfs in the data presented by Leggett et al. (2000; see their Fig. 12). Using the latter sample, Mohanty et al. (2004b) further show that the offset appears to arise from a model overluminosity in I compared to the observations. Remaining opacity uncertainties in the syn-

thetic spectra probably account for this. In particular, the F090M filter covers 0.8 – $1.0 \mu\text{m}$; in mid- to late-M and early-L dwarfs, this entire region exhibits strong FeH opacity due to the $F^4\Delta_i - X^4\Delta_i$ transition (the most prominent band of which is the 0 – 0 Wing-Ford band head at $0.9896 \mu\text{m}$; Wing & Ford 1969; Phillips et al. 1987; Kirkpatrick et al. 1999; Dulick et al. 2003). The DUSTY spectra (or any Lyon synthetic spectra for that matter), however, do not yet include any FeH opacity at $\lesssim 1 \mu\text{m}$ (F. Allard 2006, private communication), since oscillator strengths for this transition were unknown until recently. Dulick et al. (2003) have now calculated detailed line strengths and opacities for this transition, from high-level ab initio calculations of the electronic dipole transition moment. Inclusion of these new opacities could conceivably resolve the F090M (or, equivalently, I band) discrepancy observed in 2M1207A and field M dwarfs relative to the synthetic spectra.¹⁰ Moreover, FeH lines due to the $F^4\Delta_i - X^4\Delta_i$ transition extend into the J band as well (most prominently, band heads of the 0 – 1 and 1 – 2 bands at 1.1939 and $1.2389 \mu\text{m}$, respectively). It is thus possible that the J -band offset noted earlier in 2M1207A and field M dwarfs could also be fixed with the new opacities (since the FeH J -band opacities currently in the Lyon spectra are only very rough initial estimates; F. Allard 2006, private

¹⁰ An overluminosity in I is also seen in the COND models compared to T dwarfs; this is ascribed to uncertainties in the model treatment of H_2 and He collisional broadening of the far line wings of the $\text{Na}\,\text{i}$ and $\text{K}\,\text{i}$ alkali doublets (Allard et al. 2001; Baraffe et al. 2003). However, this appears unlikely to cause the I -band discrepancy in 2M1207A and field M dwarfs: the alkali doublets are much narrower in these sources than in the high-pressure atmospheres of T dwarfs. FeH uncertainties seem a better bet in this case.

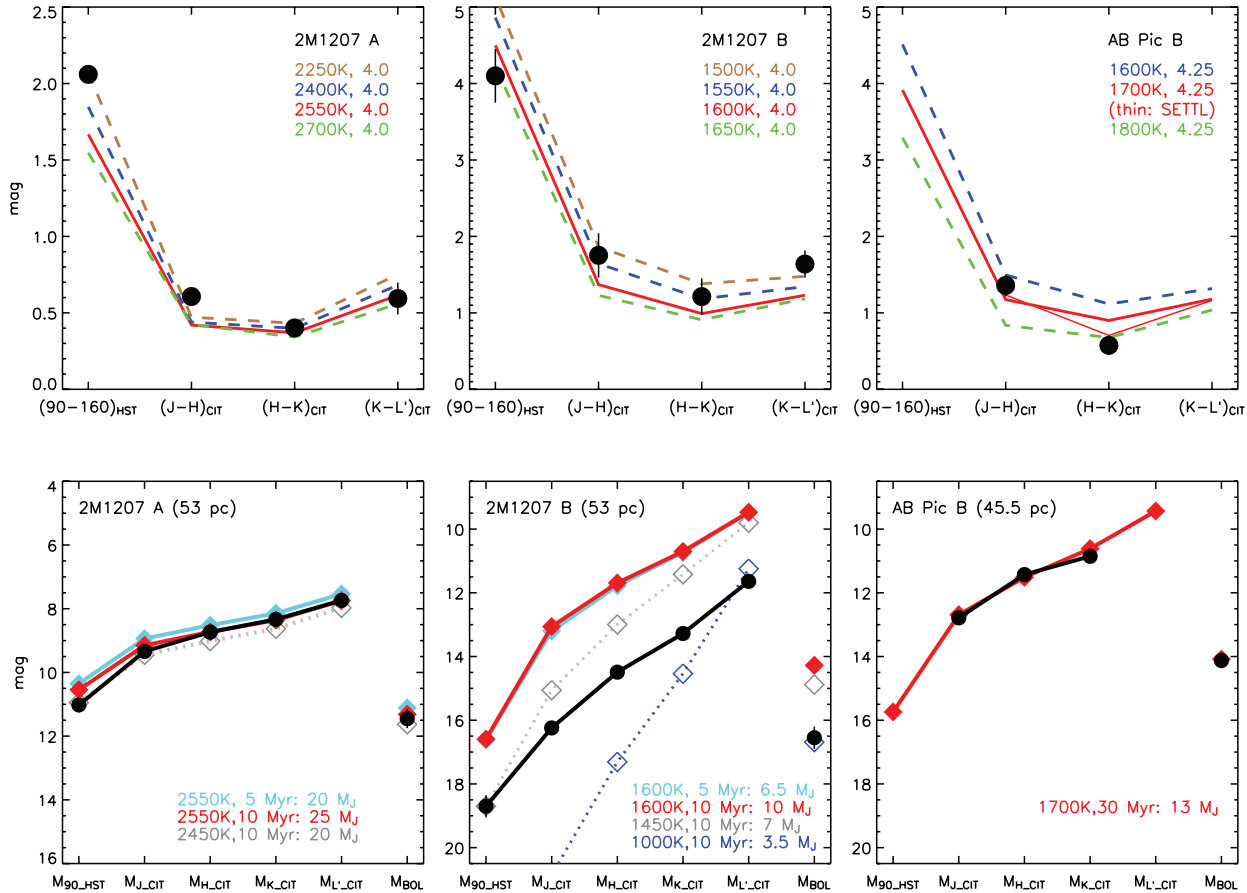


FIG. 14.—*Top panels:* Comparison of the observed colors of 2M1207A, 2M1207B, and AB Pic B to model atmosphere predictions. All models shown are DUSTY, unless otherwise noted. *Top left:* 2M1207A. Black filled circles are the data: *HST* [F090M – F160W] ($\sim I - H$) and ground-based $J - H$, $H - K$, and $K - L'$, from left to right. Models at various T_{eff} for $\log g = 4.0$ are shown as colored lines (see key in plot). *Top middle:* Same as the top left panel, but for 2M1207B. The y-axis scaling here is twice that for 2M1207A. *Top right:* Same as the top left panel, but for AB Pic B (but with only the available $J - H$ and $H - K$ data shown). Models are now for $\log g = 4.25$. The thick lines show DUSTY models at 1600, 1700, and 1800 K, while the thin red line shows a SETTL model at 1700 K. *Bottom panels:* Comparison of the SEDs and M_{bol} of 2M1207A, 2M1207B, and AB Pic B to the evolutionary model predictions. All models shown use DUSTY atmospheres. The observed photometry has been converted to absolute magnitudes using $d = 53$ pc for 2M1207A and 2M1207B and $d = 45.5$ pc for AB Pic B. *Bottom left:* 2M1207A. Black circles show the data: M_{F090M} , M_J , M_H , M_K , $M_{L'}$, and M_{bol} from left to right. Model predictions are shown for $T_{\text{eff}} = 2550$ K at 10 Myr (red) and 5 Myr (aqua) and $T_{\text{eff}} = 2450$ K at 10 Myr (gray dashed). *Bottom middle:* Same as the bottom left panel, but for 2M1207B. The y-axis scaling is the same as in the bottom left panel. Model predictions are shown for $T_{\text{eff}} = 1600$ K at 10 Myr (red) and 5 Myr (aqua); $T_{\text{eff}} = 1050$ K at 10 Myr (blue dashed); and $T_{\text{eff}} = 1450$ K at 10 Myr (gray dashed). *Bottom right:* Same as the bottom left panel, but for AB Pic B (but with only the available J , H , and K data shown). The model prediction is shown for $T_{\text{eff}} = 1700$ K at 30 Myr (red). See §§ 7.4–7.6.

communication). At any rate, given the qualitative and quantitative similarity between our results for 2M1207A and the field M dwarfs, we are justified in postulating a roughly +0.3 mag redward offset in the DUSTY [F090M – F160W] colors; this makes the 2550 ± 150 K models agree as well with the 2M1207A *HST* data as they do with its $JHKL'$ colors and *HK* spectrum.

For 2M1207B, we see that the observed [F090M – F160W] color is in very good agreement with the 1550–1600 K DUSTY models, consistent with its other colors and our spectroscopic T_{eff} of 1600 ± 100 K. The absence of any obvious offset in 2M1207B's [F090M – F160W] color from the model predictions, unlike the situation in 2M1207A, may indicate that FeH is indeed the culprit in the primary as we suggest above, since the effect of FeH opacities should weaken by the mid- to late-L type of the secondary.

In summary, our analysis so far yields a *self-consistent* picture of colors, T_{eff} , age, and mass for 2M1207A and 2M1207B: model spectra and Lyon evolutionary tracks for age = 5–10 Myr, $T_{\text{eff},A} = 2550 \pm 150$ K, $T_{\text{eff},B} = 1600 \pm 100$ K, $M_A \approx 24 \pm 6 M_{\text{Jup}}$, and $M_B \approx 8 \pm 2 M_{\text{Jup}}$ agree with all of the spectroscopic and color data available, especially after accounting for known remaining uncertainties in model opacities. The only other question is, do

the evolutionary models reproduce the absolute photometry and luminosities of both components as well?

7.5. Absolute Magnitudes, and Mass from Age-Luminosity

Using Mamajek's (2005) distance estimate of 53 ± 6 pc, the absolute photometry of 2M1207A and 2M1207B can be computed from their apparent magnitudes. Mamajek then combined the resulting M_K with the empirical K -band bolometric corrections (BC_K) for field dwarfs (Golimowski et al. 2004), to derive the bolometric luminosities of 2M1207A and 2M1207B (the errors associated with using field dwarf BC_K for these young objects are addressed further below). We compare the resulting $M_{\text{F090M},J,H,K,L'}$ and M_{bol} to the Lyon evolutionary predictions with DUSTY atmospheres.¹¹ Note that we include only the

¹¹ Chauvin et al. (2004) followed the same procedure as Mamajek (2005), but with a larger distance of 70 pc; since both Mamajek and Song et al. (2006) find a smaller distance with improved data, we do not consider the Chauvin values here. Moreover, since the Song et al. (2006) distance of 59 ± 6 pc is nearly identical to Mamajek's, our results are the same for either value; we consider only the Mamajek distance here for clarity. We discuss the Chauvin et al. (2004) and Song et al. (2006) results at the appropriate points.

F090M ($\sim I$ band) photometry from the Song et al. (2006) *HST* observations, since their F110M and F160W points are roughly equivalent to the J and H photometry already in our data set. The results are plotted in the bottom left and bottom middle panels of Figure 14 and reveal the following:

1. Primary.—The bottom left panel of Figure 14 shows the emergent SED according to the Lyon DUSTY evolutionary models, for an object at our preferred $T_{\text{eff}} = 2550$ K and age = 5 and 10 Myr, compared to $M_{\text{F090M}, J, H, K, L'}$ and M_{bol} for 2M1207A with $d = 53$ pc. We see that the 10 Myr Lyon model matches the absolute HKL' photometry and bolometric luminosity of 2M1207A remarkably well: to better than 0.05 mag in HKL' and better than 0.15 mag in M_{bol} . A slightly larger deviation of ~ 0.2 mag is seen in M_J ; similarly, a 0.4 mag deviation appears in M_{F090M} . These are precisely the offsets that cause the models to be systematically bluer than the data in $J - H$ and F090M – F160W, in the color comparisons in the top left panel of Figure 14. As discussed in §§ 7.3 and 7.4, these arise from known incompleteness in the H_2O and FeH opacities and are seen in field M dwarfs as well. As such, these deviations are not a significant cause for concern in our present analysis. For example, the bottom left panel of Figure 14 shows that a $T_{\text{eff}} = 2450$ K model matches the observed M_{F090M} and M_J very well, while being slightly fainter than the data (by ~ 0.2 mag) in $M_{H, K, L'}$ and M_{bol} : a small shift of only 100 K from our preferred T_{eff} . For the same distance, the 5 Myr model is brighter in all bands and overall luminosity by ~ 0.2 mag; however, this age can also be accommodated by a ~ 5 pc increase in distance, within the errors of Mamajek's determination. On the other hand, the $d = 70$ pc used by Chauvin et al. (2004) makes the primary brighter by 0.6 mag and significantly degrades the model fit at either age (not shown). Since Mamajek's $d = 53 \pm 6$ pc is based on space motions alone, the excellent fit it yields to the Lyon evolutionary models in our *independent* luminosity analysis makes it (and, equivalently, the very similar estimate by Song et al. 2006) the preferred distance. Changing T_{eff} by the ± 150 K uncertainty in our derivation does not appreciably alter these conclusions. Note that the associated Lyon model radius for 2M1207A, for $T_{\text{eff}} \approx 2550$ K and age = 5–10 Myr, is $\sim 0.26 R_{\odot}$. This agrees very well with the $0.24 R_{\odot}$ inferred directly from its L_{bol} and T_{eff} .

2. Secondary.—The bottom middle panel of Figure 14 depicts the same analysis for 2M1207B, using Lyon DUSTY evolutionary models at 5 and 10 Myr with our preferred $T_{\text{eff}} = 1600$ K. As expected from our prior color analysis, the Lyon models at either age reproduce the observed *shape* of the secondary's SED quite well (small deviations from the shape, apparent in F090M and L' , are discussed in § 9). However, the secondary appears *considerably fainter than predicted, by roughly the same amount in all photometric bands and bolometric luminosity*. For our preferred $d = 53$ pc, it is fainter than the models by 2.5 ± 0.5 mag in F090M, J , H , K , L' , and M_{bol} . Even for the Chauvin et al. (2004) overestimated value of $d = 70$ pc, the deviation would still be 1.9 ± 0.5 mag. Varying T_{eff} by the ± 100 K uncertainty in our derivation has a negligible impact on this conclusion.

On the other hand, for $d = 53$ pc and age 5–10 Myr, $T_{\text{eff}} \approx 1000$ K Lyon models provide a much better match to the secondary's bolometric luminosity, corresponding to masses of $3\text{--}4 M_{\text{Jup}}$. This is illustrated by the 1000 K ($4M_{\text{Jup}}$ at 10 Myr) model plotted in the bottom middle panel of Figure 14. For the Chauvin et al. (2004) value of $d = 70$ pc, a similarly good match to M_{bol} is found with $T_{\text{eff}} \approx 1250$ K ($5M_{\text{Jup}}$ at 10 Myr; not shown). This is not surprising, since the 3–5 M_{Jup} estimates by Chauvin et al.

(2004) and Mamajek (2005) were *based* on age- M_{bol} analyses. However, models at these low T_{eff} , unlike those at ~ 1600 K, fail miserably at reproducing the observed *shape* of the secondary's SED, as discussed in our earlier T_{eff} and color-color analyses. For example, note the predicted SED for the 1000 K DUSTY Lyon model in the bottom middle panel of Figure 14: far redder, and 3–5 mag fainter in J and H and 7 mag fainter in F090M, than observed (equally large deviations occur for COND or SETTL models at similar T_{eff} , with the models now being too blue and much brighter than observed in J and H ; not shown in the bottom middle panel of Fig. 14, but see discussion in § 7.1). Conversely, matching the observed absolute magnitude in, say, F090M, requires a $T_{\text{eff}} = 1450$ K model (see Fig. 14, *bottom middle panel*), which again fails entirely in fitting the SED at longer wavelengths and is also brighter than the observed M_{bol} by 2 mag.

In summary, there is a stark contrast between 2M1207A and 2M1207B. For the estimated age and distance of the system, the T_{eff} indicated by the primary's spectrum and colors also adequately reproduces its absolute photometry and bolometric luminosity. In the secondary, however, there is a serious disagreement between the T_{eff} suggested by its observed luminosity and the T_{eff} implied by its spectrum and colors.

7.6. Comparison to AB Pic B

To drive home the point that 2M1207B is indeed deviant, we have also performed the same analysis for the recently discovered young, very low mass brown dwarf AB Pic B (Chauvin et al. 2005b). The spectral type and age of this object ($\sim \text{L1-L3}$, 30 Myr), as determined by the latter authors, are roughly similar to those of 2M1207B; as such, it serves as an excellent test of our 2M1207B analysis. Our results are plotted in the right panels of Figure 14.

The top right panel of Figure 14 shows the $J - H$ and $H - K$ colors reported for AB Pic B by Chauvin et al. (2005b; we have converted to CIT from their reported 2MASS filters, as discussed in § 5), compared to DUSTY and SETTL models at $\log g = 4.25$ (the gravity indicated by the Lyon evolutionary models for brown dwarfs at ~ 30 Myr). We see that the observed $J - H$ and $H - K$ are consistent with DUSTY models at 1600–1700 K and 1800 K respectively, overall suggesting $T_{\text{eff}} \sim 1700$ K. Indeed, the 1700 K SETTL model, which is slightly bluer (by 0.2 mag) in $H - K$ than the DUSTY model at the same T_{eff} , clearly provides a good match to both the observed $J - H$ and $H - K$. We therefore adopt $T_{\text{eff}} \approx 1700 \pm 100$ K, a temperature that is very similar to the 1600 ± 100 K derived for 2M1207B.

The bluer $H - K$ in SETTL, compared to DUSTY, in the above fits deserves a word. At $\log g = 4.0$, SETTL and DUSTY spectra predict very similar $H - K$ for $T_{\text{eff}} \gtrsim 1600$ K; this is why we obtained nearly identical results from our earlier DUSTY and SETTL fits to the HK spectrum of 2M1207B. In the AB Pic B color fits, however, we employ a slightly higher gravity of $\log g = 4.25$. As discussed in § 5, the mixing scale height in the SETTL models is proportional to $(1/g)^{1/2}$ and thus decreases (implying more settling) with increasing gravity. Consequently, for a given T_{eff} , the SETTL models move closer to COND ones as gravity goes up and thus become increasingly blue in $H - K$ compared to DUSTY (for the reasons described in § 7.1.1). This is in line with observations, as follows. As noted earlier, high-gravity field L dwarfs with T_{eff} similar to 2M1207B exhibit considerable grain settling, while the much younger and lower gravity 2M1207B evinces hardly any settling at all, thus appearing redder in $H - K$ than the latest field L types. AB Pic B, again at a similar T_{eff} but slightly older and with higher gravity than 2M1207B, fits nicely into this sequence

by showing a hint of settling and thus somewhat bluer $H - K$ than 2M1207B.

We now compare the absolute JHK photometry and bolometric luminosity of AB Pic B, computed for the estimated $d = 45.5$ pc to the AB Pic system (Song et al. 2003, from *Hipparcos*¹²), to the Lyon DUSTY evolutionary predictions for $T_{\text{eff}} = 1700$ K, age = 30 Myr. Ideally, given our color results above, we should compare to Lyon models with SETTL instead of DUSTY atmospheres, but these have not yet been constructed. However, the precise atmosphere used makes very little difference to the predicted bolometric luminosity, as stated before. Moreover, the difference in predicted absolute photometry between the SETTL and DUSTY models will only be at the ~ 0.2 mag level indicated by the $H - K$ color difference in the bottom middle panel of Figure 14. For our purposes here, therefore, the available Lyon DUSTY models will suffice. The results are plotted in the bottom right panel of Figure 14. We see that the model predictions match the data extremely well, to within 0.1 mag in M_J , M_H , and M_{bol} and 0.2 mag in M_K . The slightly redder model slope from H to K , compared to the data, is precisely the difference that should be resolved by using a SETTL instead of DUSTY atmosphere.

We point out that Chauvin et al. (2005b) have also inferred $T_{\text{eff}} \sim 1700$ K for AB Pic B, by directly comparing its observed bolometric luminosity to that predicted by the Lyon evolutionary models for various T_{eff} at the system's age and distance. Our analysis has proceeded from a more fundamental level. We have first derived $T_{\text{eff}} \sim 1700$ K by comparing the observed colors to synthetic spectra and then shown that the Lyon evolutionary model for this temperature also matches the observed absolute photometry and bolometric luminosity. Our results for AB Pic B mirror those for 2M1207A; neither of these sources evinces any sign of the large deviation between models and data seen in 2M1207B.

These results are encapsulated in Figure 15, where the data are placed on the Lyon theoretical H-R diagram using $d = 53$ and 45.5 pc for 2M1207AB and AB Pic B, respectively. For 2M1207A, the age- T_{eff} , age- L_{bol} , and $T_{\text{eff}}-L_{\text{bol}}$ comparisons to the models yield completely self-consistent results: $T_{\text{eff}} \approx 2550 \pm 150$ K, $\log(L/L_{\odot}) = 2.68 \pm 0.12$, mass = $20-30 M_{\text{Jup}}$, and age = 5–10 Myr. Similarly, for its observed bolometric luminosity and our derived $T_{\text{eff}} \approx 1700$ K, AB Pic B lands nicely on the ~ 30 Myr isochrone, in complete agreement with its expected age (the associated mass is $\sim 13 M_{\text{Jup}}$). For 2M1207B, however, the results are highly divergent. Fixing age- T_{eff} yields mass $6-10 M_{\text{Jup}}$ but predicts L_{bol} 8 times higher than observed; fixing age- L_{bol} gives mass $3-4 M_{\text{Jup}}$ but T_{eff} 600 K lower than we derive; and fixing $T_{\text{eff}}-L_{\text{bol}}$ predicts age >0.5 Gyr, much older than expected for a TWA member. The agreement between models and data for 2M1207A, and particularly for AB Pic B, which is roughly similar in age, spectral type, and temperature to 2M1207B, strongly suggests that our analysis is accurate and that 2M1207B is uniquely deviant for a real physical reason.

Finally, we note that our adopted L_{bol} for all objects are derived using BC_K appropriate for field dwarfs. In particular, we use mid- to late-L field dwarf BC_K for 2M1207B. The spectrum and colors of 2M1207B, however, are much redder than in these dwarfs; i.e., its K -band flux represents a larger fraction of its total bolometric flux than in the field objects. This effect can be seen clearly in the COND/DUSTY model comparisons at various gravities shown previously in Figure 6. All of the models here

¹² Chauvin et al. (2005b) quote a slightly larger distance of 47.3 pc but do not give a reference for this value. We thus adopt the *Hipparcos* distance cited by Song et al. (2003). The small difference between the two values has no effect on our results.

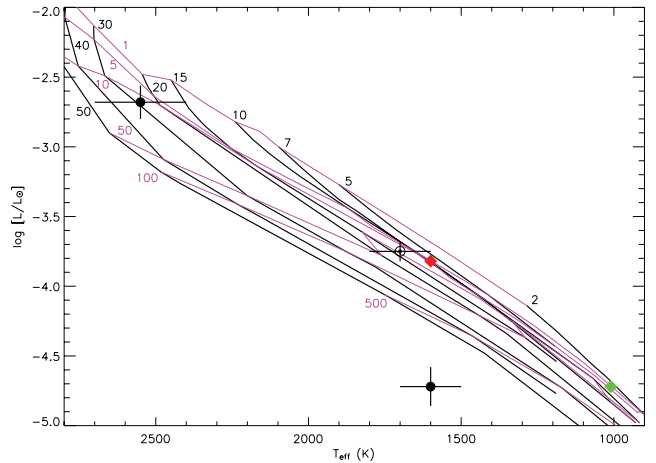


Fig. 15.—Comparison of the derived T_{eff} and L_{bol} for 2M1207A, 2M1207B, and AB Pic B to the Lyon theoretical H-R diagram. Black lines denote evolutionary tracks for masses of $2-50 M_{\text{Jup}}$ (masses marked on plot). Magenta lines denote isochrones at 1, 5, 10, 50, 100, and 500 Myr (marked on plot; age increases from top to bottom). The observed position of 2M1207A is completely consistent with a mass of $20-30 M_{\text{Jup}}$ and age of 10 Myr, in agreement with our previous results. Similarly, for its derived T_{eff} and L_{bol} , AB Pic B (bullseye) lies at its expected age of ~ 30 Myr. The T_{eff} and L_{bol} of 2M1207B, however, imply an age >0.5 Gyr, completely inconsistent with the expected 5–10 Myr. The green diamond shows that forcing 2M1207B to lie on the 5–10 Myr isochrone, for its observed L_{bol} , requires $T_{\text{eff}} \sim 1000$ K, 600 K cooler than implied by its spectrum and colors. Conversely, the red diamond shows that forcing 2M1207B to lie on the 5–10 Myr isochrone, at the derived $T_{\text{eff}} \sim 1600$ K, requires an L_{bol} nearly an order of magnitude larger than observed. See § 7.6.

have been normalized to unit area by dividing by the appropriate bolometric flux σT_{eff}^4 . We see that for a given $T_{\text{eff}} \lesssim 2000$ K, the relative K -band flux increases with decreasing gravity, in both COND and DUSTY. Moreover, for a given gravity and T_{eff} , the K -band flux in the DUSTY models is larger than in the COND ones. These effects arise from the various opacity issues discussed in § 7.1.1. Now, we have found that the colors and spectrum of 2M1207B are well matched by a low-gravity DUSTY model. Conversely, field mid- to late-L dwarfs at T_{eff} similar to 2M1207B have high gravities, as well as enhanced settling corresponding more closely to COND models. Consequently, the K -band flux in 2M1207B, relative to its bolometric flux, should indeed be higher than in field L dwarfs, due to both gravity and settling effects. Applying the dwarf BC_K , therefore, overestimates 2M1207B's observed luminosity; correcting for this should make it appear even fainter than the theoretical prediction, exacerbating all of the discrepancies cited above.

8. DISCUSSION

We consider five possible explanations for the anomalous behavior of 2M1207B:

1. Our T_{eff} is correct, but the theoretically predicted luminosity is too high because 2M1207B is much farther away or substantially older than we assume.
2. Our T_{eff} is correct, but the theoretically predicted luminosity is too high because 2M1207B's radius is smaller than the evolutionary models predict for its temperature and age (i.e., the theoretical $T_{\text{eff}}-L_{\text{bol}}$ relationship is wrong).
3. The age, distance, and theoretical $T_{\text{eff}}-L_{\text{bol}}$ relationship are correct, but the true T_{eff} is lower than the spectral models suggest, due to opacity errors in the latter.
4. The age and distance are correct, but our T_{eff} and L_{bol} are inappropriate because this is an intrinsically bluer, brighter source, heavily reddened by dust in our line of sight.

5. The age, distance, and inferred T_{eff} are all accurate, but 2M1207B appears underluminous due to *gray* extinction by a nearly edge-on disk.

We consider each possibility in turn and show that only the last is viable.

8.1. Distance and Age Uncertainties

The young age (5–10 Myr) of TWA is supported by various independent lines of evidence: presence of lithium absorption, large X-ray emission and strong chromospheric activity in its members, location of its members in the H-R diagram, and its inclusion of at least some actively accreting classical T Tauri stars (Kastner et al. 1997; Webb et al. 1999; Muzerolle et al. 2000; Zuckerman et al. 2001; Weinberger et al. 2002; Song et al. 2003; Mohanty et al. 2003; Zuckerman & Song 2004). The nearby distance (~ 40 –70 pc) to the association is supported by both trigonometric parallaxes to a few members (Perryman et al. 1997; Wichmann et al. 1998) and a moving cluster analysis based on individual space motions (Mamajek 2005). As discussed in § 1, 2M1207A exhibits several characteristics of youth consistent with TWA membership. The data reported in this paper (both the peaked H -band spectral shape and weak K -band Na I absorption indicative of low gravity, and the excellent agreement with the theoretical evolutionary tracks for an age of 5–10 Myr and $d \approx 53$ pc) provide further evidence of its youth and proximity.

If 2M1207B is physically associated with 2M1207A, it therefore cannot be farther away than ~ 50 –70 pc or significantly older than 5–10 Myr. Explaining its nearly order-of-magnitude luminosity discrepancy through distance/age variations, however, requires grossly larger values: $d \sim 150$ –200 pc and/or age > 0.5 Gyr. Since the astrometry presented by Chauvin et al. (2005a) and Song et al. (2006) implies, to a very high significance, that 2M1207A and 2M1207B indeed form a single bound system, such a large distance or age can be ruled out.

8.2. Evolutionary Model Uncertainties

Alternatively, for our adopted age and T_{eff} (and hence model-implied mass) for 2M1207B, might the radius (and thus luminosity) predicted by the evolutionary tracks be too high? Its true radius must then be ~ 3 times smaller than expected, to produce the requisite reduction in luminosity. We examine a suite of recent results to test the viability of this hypothesis.

From high-resolution spectroscopic analysis of T_{eff} and gravities, Mohanty et al. (2004a, 2004b) conclude that at very young ages (few Myr), the theoretical radii are in good agreement with observations down to masses of about $0.03 M_{\odot}$, but possibly too small by up to a factor of ~ 2 in the lowest mass brown dwarfs. These results remain to be verified through more accurate (and empirical) radius measurements; more importantly, the implied trend (true radii *larger* than predicted) is in the opposite sense to what we require.

On the other hand, Close et al. (2005) have suggested that AB Dor C, with a dynamical mass of $0.09 M_{\odot}$, is ~ 2.5 times fainter than predicted, for their adopted age of 50 Myr. Prima facie, this discrepancy is in the direction we require. However, while the Close et al. (2005) inferred mass is robust, their claim of a luminosity offset from the tracks is highly sensitive to their assumed age. Detailed analyses by Luhman et al. (2005) show that 50 Myr is too low: the true age appears to be ~ 100 Myr, removing the postulated luminosity offset.

Finally, all current empirical tests of the mass-radius relationship in stars, brown dwarfs, and planets—interferometric radius measurements of ~ 0.1 – $0.5 M_{\odot}$ field M dwarfs (Ségransan et al.

2003), eclipsing binary measurements for higher mass stars (~ 0.5 – $0.8 M_{\odot}$; Torres & Ribas 2002), very recent measurements for the first young eclipsing binary brown dwarf system (in Orion, age ~ 1 Myr, $m = 0.06$ and $0.03 M_{\odot}$; Stassun et al. 2006), and radius measurements for transiting hot Jupiters (Baraffe et al. 2005)—indicate that the theoretical radii are correct to within 25%. Moreover, in those cases where offsets exist between the models and data, the true radii are again *larger* than predicted (for various physical reasons in different mass/age/environment regimes; Baraffe et al. 2002, 2003; Chabrier et al. 2004).

In summary, all reliable evidence, from stellar to planetary masses over a range of ages, points to generally reasonable agreement between the observed and theoretical radii for a given mass; when the models err, it is by predicting sizes that are somewhat too small, instead of too big. In this light, a very large (factor of 3) *overestimation* of radius by the evolutionary tracks for 2M1207B appears untenable.

The above arguments apply if 2M1207B formed in a manner similar to an “isolated body,” i.e., conventional brown dwarf evolutionary models are appropriate. However, Fortney et al. (2005) suggest that planets formed via core accretion should be considerably smaller and fainter in their youth than standard evolutionary models predict, due to initial condition effects. While this effect may not be apparent in the transiting exoplanets discovered so far and discussed above, since they all have ages greater than or approximately a few hundred Myr, can it explain our results for the much younger 2M1207B? The answer is no: as Fortney et al. (2005) themselves point out, 2M1207B is not expected to have formed by core accretion. Calculations by Lodato et al. (2005) show why. For in situ formation of 2M1207B at its projected separation from the primary (~ 40 AU for $d \sim 53$ pc), in the available time ($\lesssim 10$ Myr), the required disk surface density for core accretion translates to a disk mass far too large to be entertained. Core accretion much closer to the primary followed by outward migration is also not possible, since plausible timescales and disk masses require formation at disk radii < 0.6 AU, which would cause *inward* migration. With formation by core accretion ruled out, we find no compelling physical rationale for postulating a grossly overestimated radius for 2M1207B.

Lastly, is it possible that the predicted luminosity for 2M1207B is too high due to errors in the theoretical mass- T_{eff} relationship, instead of in mass-radius? In particular, consider the implications if the predicted mass-radius relation is fairly accurate (as the studies above strongly suggest), but the mass- T_{eff} relation is too cool; i.e., for a given mass and age, the evolutionary tracks indicate the correct radius but too low a temperature. For an *empirically* determined mass, of course, this would underestimate the true luminosity. However, we *derive* the mass of 2M1207B from age- T_{eff} comparisons to the theoretical tracks, using a temperature independently inferred from fits to synthetic spectra. Assuming that our T_{eff} is in the right ballpark (as we argue in § 8.3) and our adopted age is valid, a mass- T_{eff} relationship that is too cool will lead us to derive too high a mass to match our (correct) T_{eff} , and thus too large a radius. Consequently, the predicted luminosity will be too high; can this explain our results? The answer is no. Our mass for 2M1207B is already below the deuterium-burning boundary ($\sim 12 M_{\text{Jup}}$) and will be even lower if, as implied in the above scenario, the mass is actually overestimated. At an age of 5–10 Myr, the theoretical mass-radius relationship indicates that objects near and below the *D*-burning boundary all have very similar radii, with masses from $0.5 M_{\text{Jup}}$ to $15 M_{\text{Jup}}$ differing by $< 50\%$ in radius (Baraffe et al. 2003). Hence, the luminosity will be overestimated by no more than a factor of ~ 2 , far too small to explain the nearly order-of-magnitude discrepancy seen in 2M1207B.

This conclusion becomes even stronger if, as Mohanty et al. (2004b) and Stassun et al. (2006) suggest, the theoretical radii at young ages are somewhat underestimated for low substellar masses, since this would make the luminosity overprediction in the above scenario even smaller.

In conclusion, radius or T_{eff} errors in the evolutionary models are not a plausible explanation for 2M1207B appearing vastly fainter than predicted. From an empirical standpoint, the remarkably good match between the theoretical and observed luminosities in both 2M1207A and AB Pic B also argues strongly against serious problems in the evolutionary models. The evidence from AB Pic B is especially compelling, since it has a roughly similar spectral type and nearly the same T_{eff} , from synthetic color comparisons, as 2M1207B, while being only slightly older. Consequently, its expected mass and luminosity from age- T_{eff} model comparisons are close to the values predicted for 2M1207B. As such, it is hard to imagine a missing piece of evolutionary physics that generates a very large difference between the predicted and observed luminosities in 2M1207B but causes no such offset in AB Pic B.

8.3. Atmospheric Model Uncertainties

Another possibility is that the theoretical $T_{\text{eff}}-L_{\text{bol}}$ relationship is correct, but it is the atmospheric models that are wrong: erroneous opacities cause us to infer, from both our spectral and color analyses, T_{eff} too high by ~ 600 K. Without other young ultracool objects with *empirically* determined T_{eff} , we cannot test this proposition directly. However, four lines of evidence argue strongly against such large errors in the atmospheric models.

The first is a qualitative argument. Matching the observed bolometric luminosity of 2M1207B, at its age and distance, requires $T_{\text{eff}} \sim 1000$ K (§ 7.5). Conversely, atmospheric models over a narrow but much higher range of T_{eff} , 1600 ± 100 K, reproduce very well both its *HK* spectral shape and, independently, its $\sim I$ to L' colors. This large wavelength coverage includes opacities from a number of different sources, e.g., H₂O, H₂-CIA, TiO, and dust grains. Errors in all of these opacities would have to be very finely tuned, indeed, for the models at ~ 1600 K to fortuitously reproduce precisely the same spectral shape and colors appropriate to a ~ 600 K lower temperature, over the entire *IJHKL'* range. Instead, any severe opacity errors are more likely to yield very *divergent* T_{eff} estimates from the different color and spectral comparisons. This is not seen in our analysis and suggests that the synthetic spectra are not too far off the mark in their temperature prediction.

An examination of $K-L'$ colors provides a second, more compelling argument. The $K-L'$ colors of field M, L, and T dwarfs are known to form a tight monotonically increasing sequence with decreasing T_{eff} , despite the range in age and dust properties encompassed by these sources (Golimowski et al. 2004). This is illustrated in Figure 16, where we plot $K-L'$ in MLT dwarfs against their semiempirically derived “structural” T_{eff} (data from Golimowski et al. 2004; T_{eff} via parallax, flux-calibrated spectra, and theoretical $T_{\text{eff}}-L_{\text{bol}}$ relationship; see latter paper for details).¹³ The T_{eff} errors are roughly ± 150 K for sources with imprecise

¹³ From the Golimowski et al. (2004) sample, we have excluded those sources (1) known (or suspected by Golimowski et al. 2004) to be unresolved binaries, since the L_{bol} , T_{eff} , and colors of the individual components are not well determined and those of the combined systems are prone to systematic offsets from single dwarfs (Liu & Leggett 2005); (2) for which Golimowski et al. (2004) estimate L' flux by extrapolation from *JHK* photometry and spectral type, since these estimates have large errors, leading to higher uncertainties in L_{bol} and T_{eff} than in sources with directly measured L' flux; and (3) for which NIR and optical spectral types differ by >1 subtype, when classifications are available in both, since these may be anomalous.

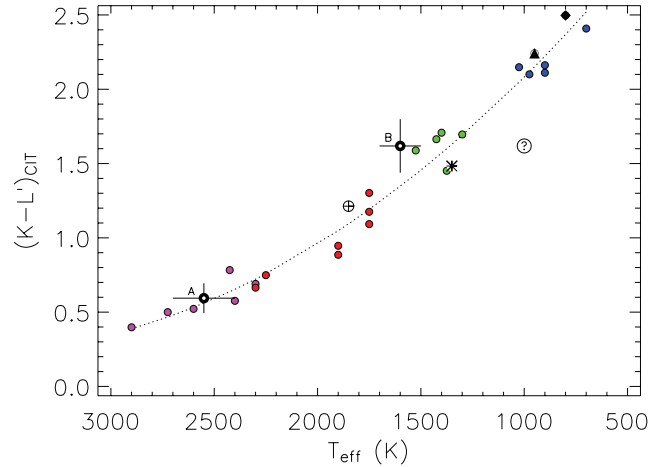


FIG. 16.—Empirical $K - L'$ vs. T_{eff} relationship in field M, L, and T dwarfs. The dwarfs are shown by filled circles: mid to late M (M6–M9.5) in magenta; early to mid L (L0–L5.5) in red; late L to early T (L6–T3) in green; and mid to late T (T4–T9) in blue. The photometry errors for the field dwarfs are generally comparable to the symbol sizes. The T_{eff} shown assume a median age of 3 Gyr. A few well-known dwarfs with independent age estimates are shown by special symbols: GD 165B (L3, circled crosshairs), GI 584C (L8, asterisk), GI 229B (T6, filled triangle), and GI 570D (T8, filled diamond). The field dwarfs form a tight monotonically increasing sequence in $K - L'$ with decreasing T_{eff} ; the dotted line shows a second-order polynomial fit to the data to guide the eye. Finally, 2M1207A and 2M1207B are also plotted, as bull’s-eyes, at their observed $K - L'$ and the T_{eff} derived from our spectral and color analysis. The position of both sources is fully consistent with the empirical field dwarf sequence. The circled question mark denotes the position of 2M1207B if its T_{eff} were actually 1000 K, as required to match its L_{bol} but 600 K cooler than we derive; this would clearly make it a significant outlier from the field dwarf color- T_{eff} sequence shown. See § 8.3.

ages and ± 100 K for better constrained ages.¹⁴ The plot clearly shows the monotonic color sequence with T_{eff} .¹⁵ We emphasize that this trend is *independent* of any atmospheric modeling.

Now we examine 2M1207A and 2M1207B on the same plot. Their observed $K - L'$ colors and the T_{eff} we *derive* from the atmospheric models clearly place both sources firmly within the empirical field dwarf sequence. In particular, adopting T_{eff} lower by ~ 600 K than our estimate would make 2M1207B a significant outlier (even after accounting for the ± 150 K uncertainty in the field dwarf temperatures). This further supports our inferred T_{eff} . Moreover, our T_{eff} for 2M1207A and 2M1207B (2550 ± 150 K and 1600 ± 100 K, respectively) place them precisely in the regions of the diagram expected for their approximate spectral types: late M and mid to late L, respectively. This is another indication that our temperatures are in the right ballpark.

AB Pic B provides the third argument. Using model atmospheres with $\log g = 3.5–4.5$, we find $T_{\text{eff}} = 1600 \pm 100$ K for 2M1207B. With a gravity in the same range, $\log g = 4.25$, we

¹⁴ For dwarfs with imprecise ages, Golimowski et al. (2004) conservatively assume 0.1–10 Gyr. For a handful of the dwarfs in resolved multiple systems, ages are better constrained by assuming coevality with the main-sequence primaries. These are GD 165B (1.2–5.5 Gyr), GI 584C (1–2.5 Gyr), GI 570D (2–5 Gyr), and GI 229B (0.5–10 Gyr) (Golimowski et al. 2004 and references therein).

¹⁵ Golimowski et al. (2004) and Leggett et al. (2002b) have noted that $K - L'$ levels out over the spectral type range L6–T5, although it rises with later type on both sides of this interval. However, Golimowski et al. (2004) also find that the structural T_{eff} corresponding to L6–T5 is roughly constant ($\sim 1300–1500$ K). Consequently, $K - L'$ rises much more monotonically with T_{eff} than with spectral type, as evinced by our plot (all of the L6–T5 sources are bunched together at nearly the same T_{eff} and $K - L'$; green circles and asterisk in Fig. 16). As Golimowski et al. (2004) discuss, the constancies of both T_{eff} and $K - L'$ over the L6–T5 interval are probably related, arising from dust-settling and cloud-clearing phenomena in these field L–T transition objects.

derive a very similar temperature, ~ 1700 K, for AB Pic B as well. If severe synthetic opacity errors cause us to overestimate T_{eff} in 2M1207B by ~ 600 K, then the same should hold for AB Pic B too, i.e., the latter should also appear severely underluminous compared to the evolutionary tracks. The fact that it does not bolster our confidence in the T_{eff} inferred for 2M1207B, since we use the same atmospheric models for the temperature analysis of both.

Our final argument is based on the temperatures of field MLT dwarfs. A number of these have T_{eff} estimated from spectral modeling, as well as semiempirical structural T_{eff} derived from their empirical L_{bol} combined with the theoretical $T_{\text{eff}}-L_{\text{bol}}$ relationship for field ages (Dahn et al. 2002; Golimowski et al. 2004; Vrba et al. 2004). These structural T_{eff} , while still dependent on the evolutionary models, are our best current estimates of the true temperatures of these dwarfs. Comparing them to the spectroscopic T_{eff} indicates the following systematics in the latter (see also Smith et al. 2003). For mid-M dwarfs, where dust formation is marginal, the spectroscopic T_{eff} seem systematically too cool by ~ 200 K. This is ascribed to remaining lacks in the NIR model H₂O opacities at these relatively hot temperatures (Leggett et al. 2001). Conversely, in the late-L to early-T dwarfs, where ongoing dust settling is a major phenomenon, the spectroscopic T_{eff} appear too hot by ~ 200 K (e.g., Schweitzer et al. 2002). This is because nearly all comparisons to these sources have been on the basis of inappropriate no-settling (i.e., DUSTY) or fully settled (i.e., COND) model conditions; new models that do incorporate partial settling (e.g., SETTL) now show marked improvements in this regime (e.g., Allard et al. 2003a; Knapp et al. 2004; Burrows et al. 2006). On the other hand, in late-M to mid-L dwarfs, where dust remains fully suspended in the atmosphere, and mid- to late-T dwarfs, where dust has entirely settled below the photosphere, the spectroscopic T_{eff} agree quite well with the structural ones, with a scatter of order the ~ 100 – 200 K uncertainty in the latter (e.g., Leggett et al. 2001, 2002a; Schweitzer et al. 2001; Allard et al. 2003b; Burrows et al. 2006). Hence, given the very dusty photosphere indicated by the extreme red colors and spectrum of 2M1207B and the good agreement between spectroscopic and structural T_{eff} in the fully DUSTY regime, we do not expect a systematic error in excess of 100– 200 K in our T_{eff} for 2M1207B. Moreover, we have seen that in both 2M1207A and AB Pic B, the luminosities implied by combining the theoretical $T_{\text{eff}}-L_{\text{bol}}$ relationship with our spectroscopic T_{eff} match the observed luminosities very well, within the 100– 150 K uncertainty in our temperature determination. This too implies that our T_{eff} systematics is $\lesssim 150$ K.

The combined weight of the above suggests that, while we cannot rule out 100– 200 K systematics in our T_{eff} for 2M1207B, due to model opacity uncertainties, it is highly implausible that we are overestimating T_{eff} by the ~ 600 K required to match its observed luminosity.

8.4. Interstellar Extinction

Yet another possibility is that 2M1207B is intrinsically bluer and brighter than observed, but heavily reddened by dust in our line of sight. While this would not affect age or distance, it would nullify the T_{eff} and L_{bol} we derive assuming negligible extinction and reddening.

Large interstellar extinction toward a TWA member is extremely unlikely, however. The association is far from any known molecular cloud that could cause significant reddening; it is also very nearby, implying very little intervening interstellar medium dust. In keeping with this, the extinction toward the eponymous T Tauri star TW Hydra, as measured from H I absorption in Ly α

emission assuming an interstellar gas-to-dust ratio, is completely negligible (Herczeg et al. 2004). Lastly, no significant extinction is apparent in 2M1207A (as indicated by the excellent match of its SED and absolute photometry to the evolutionary models, assuming zero reddening; Fig. 14), which is located only $\sim 0.8''$ from the secondary. We can thus confidently reject interstellar reddening as the cause of 2M1207B's anomalous behavior.

8.5. Edge-on Disk

The last explanation we consider, and the simplest one consistent with our observations, is that 2M1207B suffers from *gray* extinction due to an edge-on disk. In the optically thick edge-on case, the disk obscures the central object entirely, and at short (optical and NIR) wavelengths we only see starlight scattered from the disk surfaces: a small fraction of the true luminosity of the central source. The SED of this reflected light will closely match the intrinsic spectrum of the source (see discussion further below), yielding the correct T_{eff} from spectral and color analyses, but the object will appear considerably subluminous. The net effect is of approximately gray extinction out to NIR wavelengths, as we observe.

Optically thick edge-on disks have now been imaged around a number of T Tauri stars (e.g., Burrows et al. 1996; Stapelfeldt et al. 1997, 1998; Padgett et al. 1999; Throop et al. 2001). The diminution of luminosity in these cases, relative to the intrinsic brightness estimated for the central sources, is comparable to the $\sim 2.5 \pm 0.5$ mag subluminosity we find in 2M1207B.¹⁶ For example, in the two prototypical edge-on T Tauri systems HH 30 and HK Tau/c, the observed K -band fluxes are 3–4 mag lower than expected for their age, distance, and M0–M2 spectral types (Burrows et al. 1996; Stapelfeldt et al. 1998; Monin et al. 1998; Kenyon et al. 1998; this does not of course signify the true extinction in K in these edge-on systems, which is extremely large, but is simply a measure of the scattered-to-intrinsic flux ratio). Edge-on disks have also been proposed for some objects near and below the substellar boundary, on similar luminosity grounds (Barrado y Navascués et al. 2004; Luhman 2004). Finally, the T Tauri system KH 15D exhibits periodic eclipses, with depths of ~ 3.5 mag and gray extinction of the star; this is modeled as occultation by an edge-on precessing ring or disk, with only scattered light seen during the eclipses (Herbst et al. 2002; Agol et al. 2004; Winn et al. 2004; Chiang & Murray-Clay 2004; Knacke et al. 2004; Kusakabe et al. 2005). These data support the viability of an edge-on disk for explaining our results.

The disk hypothesis is also supported by analogy with the primary in the 2M1207 system. As discussed in § 1, not only is 2M1207A already known to be surrounded by an accretion disk, but there is evidence that its disk is seen at a relatively high inclination angle, i.e., closer to edge-on than face-on, with $i \gtrsim 60^\circ$ (Scholz et al. 2005; Scholz & Jayawardhana 2006).¹⁷ It does not stretch the imagination, then, to propose that the secondary has a disk as well, seen even closer to edge-on.

Is gray extinction expected from an edge-on disk? As a star+disk system approaches an edge-on geometry, all wavelengths are attenuated due to absorption by disk dust, but shorter wavelengths are attenuated more. At large enough inclinations, the optical depth through the disk is too high for the shorter wavelengths

¹⁶ As discussed in § 7.6, the true underluminosity of 2M1207B is likely even larger than our nominal estimate using field dwarf BC_K, since the latter tend to overestimate the observed L_{bol} for this young object.

¹⁷ Note that we do not see any underluminosity in 2M1207A, arguing against a truly edge-on configuration. This remains compatible with the relatively high inclination suggested by Scholz et al. (2005), as discussed in § 9.

to make it through at all; at this point, the star is seen at these wavelengths only in scattered light, which is minimally affected by further changes in inclination. Longer wavelengths continue to reach us directly through the disk, albeit increasingly attenuated, to still higher inclinations, until, very close to edge-on, they too cannot pass through the disk anymore and are observed only via scattering off the disk surface. Consequently, any given optical or infrared color first becomes redder with increasing inclination and then reverses blueward again very close to edge-on (Whitney et al. 1997). Detailed calculations of class II T Tauri star+disk systems by Whitney et al. (2003) show that in almost perfectly edge-on cases, the star is seen entirely in scattered light out to NIR wavelengths. While the observed colors predicted by Whitney et al. (2003) for this situation are slightly bluer than the intrinsic stellar ones, due to scattering by small grains, the difference is quite small, at most a few tenths of a magnitude in the NIR. Modeling of brown dwarf disks by Walker et al. (2004) yields very similar results.

These theoretical calculations imply that an optically thick edge-on disk can indeed produce nearly gray extinction into the NIR. Moreover, with observational errors in photometry of a few tenths of a magnitude, as in 2M1207B, any minor blueing of the intrinsic starlight by scattering off small grains would be masked, and the extinction would be indistinguishable from gray (see also § 9). Observed edge-on T Tauri systems support this conclusion. For instance, LkH α 263C (MBM 12A 3C), an M0 star with an almost perfectly edge-on disk, is seen only in scattered light out to the K band, and the detected NIR colors are precisely those expected intrinsically from an M0 star (Jayawardhana et al. 2002). That is, to within the observational uncertainties in photometry, the NIR extinction in LkH α 263C is wavelength independent (i.e., gray).

The above arguments apply to optically thick edge-on disks. Alternatively, the disk may not be optically thick: large grains in an optically thin edge-on disk may occlude most of the starlight but allow some ($\sim 10\%$ in our case) to pass through. In this case, reddening due to absorption by disk grains, and blueing due to scattering, can be negligible (producing gray extinction) if the grains are substantially larger than the observed wavelengths. For 2M1207B, where the extinction appears roughly achromatic out to L' , this implies grain sizes $\gg 4 \mu\text{m}$. Gray extinction due to similarly large grains has now been established in at least one T Tauri system: in the edge-on system KH 15D, the constancy of the spectrum and colors in and out of eclipse out to the K band and the very weak polarization within eclipse imply scattering by disk/ring grains with sizes $\gg 2 \mu\text{m}$ (Agol et al. 2004; Kusakabe et al. 2005). In addition, mid-IR photometry of our primary, 2M1207A, reveals a flat disk and negligible silicate emission from small surface grains, suggesting significant grain growth and/or settling (Sterzik et al. 2004; Gizis et al. 2005a). It is not unlikely, then, that grains have grown large in the secondary's disk as well.

In summary, our analysis suggests that gray extinction due to a nearly edge-on disk is a viable explanation, and indeed the most plausible one, for the observed underluminosity of 2M1207B. The information at hand is insufficient to pin down the precise disk inclination or grain sizes; however, polarization studies, currently underway, should illuminate these issues.

9. CONCLUSIONS

The discovery of 2M1207B, an ultracool and apparently planetary mass body orbiting a nearby young brown dwarf, has been tremendously exciting from a number of standpoints. It offers us

the first chance to study the atmosphere and evolution of ultracool, planetary mass substellar objects in their infancy, the formation mechanism of the lowest mass brown dwarfs, and the extension of substellar binarity into the planetary mass domain. Initial studies of 2M1207B by Chauvin et al. (2004) and Mamajek (2005), however, point to a discrepancy between its colors and approximate spectral type on the one hand and the T_{eff} implied by its luminosity on the other: the latter seems too low. We have investigated this conundrum with new VLT NIR spectra and photometry of 2M1207A and 2M1207B.

Our analysis shows that 2M1207B is considerably underluminous for its temperature, age, and distance. In particular, it appears to suffer from roughly gray extinction of ~ 2.5 mag, in all observed bands from $\sim I$ to L' and in M_{bol} . It is this anomalous faintness that is responsible for the low T_{eff} and mass derived in earlier studies. The most plausible explanation is that 2M1207B is surrounded by a nearly edge-on disk, which occludes most (or all) of the direct light from the object and allows us to see it only in light scattered off the disk surface. This hypothesis is compatible with observations of edge-on T Tauri systems, as well as with the known presence of a high-inclination disk around 2M1207A.

Our edge-on disk proposal raises some questions. First, why does a high-inclination disk lead to underluminosity in only the secondary and not in the primary? There are two possible answers. The first is that only a small deviation from a perfectly edge-on configuration can allow us to see the primary unocculted, if its disk has an inner hole. For example, for a geometrically flat disk and an inner hole ~ 5 stellar radii in size, the primary will remain unobstructed for inclinations up to $i \sim 80^\circ$. The primary's disk is known to be quite flat from SED analyses mentioned earlier. Similarly, an inner hole of a few stellar radii, in an accretor such as 2M1207A, is compatible both with magnetospheric disk accretion models and with the inner hole sizes inferred from the observed SEDs of other substellar accretors (Liu et al. 2003; Mohanty et al. 2004c). Since the H α studies of 2M1207A simply indicate $i \gtrsim 60^\circ$ and not necessarily an exactly edge-on geometry, this explanation is consistent with our proposal. Of course, this requires that the primary and secondary disks not be exactly coplanar: edge-on in the latter, but not quite in the former. Non-coplanar disks are known in at least some binary T Tauri systems (e.g., Monin et al. 2006), so a small difference (of order 10° – 20°) in the disk orientations in 2M1207AB is not infeasible. We also recall that the separation between the 2M1207 components, as mentioned in § 1, is unusually large in the context of substellar binaries. This may point to dynamical perturbations in the past; while purely speculative, such a perturbation could misalign the component disks. On the other hand, it may be that the 2M1207B disk is not strictly edge-on either, but is instead significantly more flared than in 2M1207A, causing occultation in the former but not in the latter for the same (high) inclination angle. Models by Walker et al. (2004) of brown dwarf disks do predict greater flaring with decreasing substellar mass (because the central gravity decreases), and we cannot rule out this possibility.

Second, what other observational signatures do we expect from the 2M1207B disk that might allow us to confirm its presence? As mentioned earlier, scattering by small surface grains can cause a blueing of the starlight; conversely, at long enough wavelengths, the disk emission itself, consisting of reprocessed starlight, should begin to dominate and produce excess emission. As discussed, disk modelings indicate that both effects can be quite small (leading to simply gray extinction) for a perfectly edge-on case, at least out to NIR wavelengths, especially if grains are large and/or in the presence of multiple scattering. We have seen that these effects

are indeed not obvious in our data: within the errors, the underluminosity in all bands is consistent with being gray. Nevertheless, there are tantalizing hints of nongrayness at the longest and shortest bands. In particular, the underluminosity in JHK is $\sim 2.5 - 3$ mag, while in F090M ($\sim I$) and L' it is ~ 2.2 mag. This is why 2M1207B appears slightly redward of the model predictions in $K - L'$ in Figure 13 and the top middle panel of Figure 14. Similarly, the slight relative overbrightness in F090M, compared to JHK , is apparent in the small deviation in F090M from the overall predicted SED shape in the bottom middle panel of Figure 14 (this comparative overbrightness in F090M has also been noted by Song et al. 2006). Given the uncertainties of 0.1–0.3 mag in the photometric data, these shifts are at a $\sim 2\sigma$ level and hence not ironclad. If true, however, they point to a small blueing at the shortest wavelengths and a small red excess at the longest, consistent with disk expectations. Spatially resolved photometry of the system at still longer wavelengths, e.g., in the M band, should reveal any disk excess emission more clearly. Similarly, scattering by disk grains should produce a detectable polarization signature of at least a few percent. These observations can confirm the presence of a disk; polarization studies can further offer insights into the grain sizes and disk orientation.

Third, what is the disk mass we expect for 2M1207B, and is this consistent with the disk-to-star mass ratios seen in the stellar/substellar regimes? Unfortunately, without either a spatially resolved image of the disk or any optically thin disk emission data (e.g., in the millimeter), we cannot make any good estimates of disk mass based on our current data alone. A very rough estimate can be acquired, however, from naive opacity arguments. Assume a flat disk with radius R_d ; average thickness $2r_*$, where r_* is the radius of 2M1207B (i.e., seen edge-on, the disk is just wide enough to cover the face of the central object); and average density ρ_d . Assume further a disk grain emissivity of $\kappa_\nu = 0.1(\nu/10^{12} \text{ Hz})^\beta$ (Beckwith et al. 1990). Now imagine a radial line of sight through the edge-on disk toward 2M1207B. For the disk to be optically thick along this line of sight at a given wavelength, we must have $\tau \sim \rho_d \kappa_\nu R_d > 1$. Assuming $\tau \sim 1$ then implies a lower limit on disk density, $\rho_d \sim 1/(\kappa_\nu R_d)$, and a corresponding disk dust mass of $M_{\text{dust}} \sim 2\pi R_d r_* / \kappa_\nu$. Adopting an emissivity exponent $\beta \sim 1$ (Beckwith et al. 1990), fiducial NIR wavelength of $\sim 2.2 \mu\text{m}$ (K band), $r_* = 0.15 R_\odot$ (the radius predicted by the evolutionary models for a $\sim 8M_{\text{Jup}}$ object at ~ 10 Myr), and $R_d = 10$ AU (consistent with a tidal truncation radius for the mass ratio and [projected] separation between the components) then implies $M_{\text{dust}} \sim 7 \times 10^{23} \text{ g} \sim 0.01 M_{\text{Moon}}$. Assuming a standard gas-to-dust ratio of 100, the total disk mass is then $M_{\text{disk}} \sim 1 M_{\text{Moon}}$; the disk-to-star ratio is thus $\sim 4 \times 10^{-6}$. This can be compared to the average disk-to-star mass ratios, in the classical T Tauri stellar and substellar regimes, of $\sim 10^{-2}$ (e.g., Scholz et al. 2006). This calculation is obviously very simplistic; nevertheless, it qualitatively illustrates that a very small disk mass, fully admissible within the context of substellar disks, can occult 2M1207B.

A final implication of our results concerns the formation of the 2M1207AB system. Assuming a distance of 70 pc, Chauvin et al. (2004) originally estimated a projected component separation of ~ 55 AU and a secondary mass of $\sim 5M_{\text{Jup}}$, implying a component mass ratio of ~ 0.2 . Lodato et al. (2005) then pointed out that this separation and mass ratio are commensurate with the values observed in higher mass, *stellar* binaries. They also showed that the standard core accretion mechanism of planet formation cannot produce a $5M_{\text{Jup}}$ secondary in this system, at the observed separation: to do so in the available time ($\lesssim 10$ Myr, the age of the

system) would require far too massive a disk around the primary (at least hundreds of M_{Jup} , more than an order of magnitude heavier than the primary itself). Both facts led Lodato et al. (2005) to suggest that the 2M1207AB system probably formed in a manner akin to stellar binaries; they proposed disk fragmentation by gravitational instabilities as the most viable such mechanism. Now, our analysis of the primary's absolute photometry shows that a distance of 53 ± 6 pc, as derived by Mamajek (2005), is more appropriate for 2M1207AB, implying a projected component separation of ~ 40 AU. Our inferred secondary mass of $\sim 8M_{\text{Jup}}$ further indicates a component mass ratio of ~ 0.3 . Compared to the Chauvin et al. (2004) results, our values are even more compatible with the separations and mass ratios observed in stellar binaries (see Fig. 1 of Lodato et al. 2005). Similarly, our higher mass for 2M1207B makes its formation through core accretion even less likely. Our results thus strengthen the case for a binary-like origin for the 2M1207AB system, perhaps via gravitationally induced disk fragmentation. As Lodato et al. (2005) point out, the latter mechanism still requires the primary to have started out with a disk at least as massive as the secondary, i.e., $M_{\text{disk}} \gtrsim 0.3M_{\text{primary}}$. This is an order of magnitude higher than the disk masses currently inferred, from submillimeter/millimeter fluxes, for brown dwarfs that are ~ 1 to a few Myr old ($M_{\text{disk}}/M_{\text{BD}}$ of roughly a few percent; Klein et al. 2003; Scholz et al. 2006). However, disk masses do decline with time; while stellar T Tauri disks, at a few Myr, also contain only a few percent of the mass of the central star, disks around younger embedded protostars comprise a large fraction of the central mass. Hence, a relatively massive disk around 2M1207A much earlier in its life, when fragmentation is believed to occur, is not entirely implausible.

Lastly, it is important to remember that while our mass for 2M1207B exceeds the estimates of Chauvin et al. (2004) and Mamajek (2005), it is still in the planetary regime. It is fascinating to imagine that stellar binary formation mechanisms, when translated to the low-mass substellar domain, may directly form planetary mass companions to brown dwarfs. Our data moreover indicate that such companions can even possess disks of their own, perhaps, we speculate, capable of forming planetesimals, moons, and asteroids. Further study of 2M1207AB promises rich insights into substellar formation, evolution, and properties.

We would like to express our gratitude to the staff of ESO VLT and especially to Nancy Ageorges for her technical support and advice. S. M. would like to sincerely thank Gael Chauvin for advice on data reduction and very helpful inputs on the results, Frank Marchis for an independent deconvolution of our J -band images and a check on our photometry, Adam Burgasser and Gilles Chabrier for their suggestions and close examination of the analysis, and Kevin Luhman and Gibor Basri for many illuminating discussions that shaped this paper. We are particularly indebted to Derek Homeier, France Allard, Isabelle Baraffe, Peter Hauschildt, and Didier Saumon for providing exhaustive synthetic spectra and evolutionary models at all hours of day and night and invaluable input on atmospheric behavior. We also thank Adam Burgasser for an extremely helpful and detailed referee report. S. M. is grateful as well to the Spitzer Fellowship program for funding this research; the work was also supported in part by University of Toronto start-up funds to R. J. Finally, E. M. is supported through a Clay Postdoctoral Fellowship from the Smithsonian Astrophysical Observatory.

REFERENCES

- Ackerman, A., & Marley, M. 2001, *ApJ*, 556, 872
- Agol, E., Barth, A., Wolf, S., & Charbonneau, D. 2004, *ApJ*, 600, 781
- Allard, F., Guillot, T., Ludwig, H.-G., Hauschildt, P. H., Schweitzer, A., Alexander, D. R., & Ferguson, J. W. 2003a, in IAU Symp. 211, Brown Dwarfs, ed. E. Martín (San Francisco: ASP), 325
- Allard, F., Hauschildt, P. H., Alexander, D. R., Tamai, A., & Schweitzer, A. 2001, *ApJ*, 556, 357
- Allard, F., Hauschildt, P. H., & Schwenke, D. 2000, *ApJ*, 540, 1005
- Allard, N., Allard, F., Hauschildt, P. H., Kielkopf, J., & Machin, L. 2003b, *A&A*, 411, L473
- Baraffe, I., Chabrier, G., Allard, F., & Hauschildt, P. 2002, *A&A*, 382, 563
- Baraffe, I., Chabrier, G., Barman, T., Allard, F., & Hauschildt, P. 2003, *A&A*, 402, 701
- Baraffe, I., Chabrier, G., Barman, T., Selsis, F., Allard, F., & Hauschildt, P. 2005, *A&A*, 436, L47
- Barrado y Navascués, D., Mohanty, S., & Jayawardhana, R. 2004, *ApJ*, 604, 284
- Beckwith, S., Sargent, A., Chini, R., & Güsten, R. 1990, *AJ*, 99, 924
- Borysow, A., Jørgensen, U., & Zheng, C. 1997, *A&A*, 324, 185
- Bouy, H., Brandner, W., Martín, E., Delfosse, X., Allard, F., & Basri, G. 2003, *AJ*, 126, 1526
- Bouy, H., Martín, E., Brandner, W., Zapatero-Osorio, M. R., Béjar, V. J. S., Schirmer, M., Huélamo, N., & Ghez, A. M. 2006a, *A&A*, 451, 177
- Bouy, H., Moraux, E., Bouvier, J., Brandner, W., Martín, E. L., Allard, F., Baraffe, I., & Fernández, M. 2006b, *ApJ*, 637, 1056
- Brandeker, A., Jayawardhana, R., & Najita, J. 2003, *AJ*, 126, 2009
- Burgasser, A. 2004, *ApJS*, 155, 191
- Burgasser, A., Kirkpatrick, D., Reid, N., Brown, M., Miskey, C., & Gizis, J. 2003a, *ApJ*, 586, 512
- Burgasser, A., Marley, M., Ackerman, A., Saumon, D., Lodders, K., Dahn, C. C., Harris, H. C., & Kirkpatrick, J. D. 2002, *ApJ*, 571, L151
- Burgasser, A., et al. 2003b, *ApJ*, 592, 1186
- Burrows, A., & Liebert, J. 1993, *Rev. Mod. Phys.*, 65, 301
- Burrows, A., Sudarsky, D., & Hubeny, I. 2006, *ApJ*, 640, 1063
- Burrows, C., et al. 1996, *ApJ*, 473, 437
- . 1997, *ApJ*, 491, 856
- Carpenter, J. 2001, *AJ*, 121, 2851
- Chabrier, G., Allard, F., Baraffe, I., Barman, T., & Hauschildt, P. 2004, in ASP Conf. Ser. 321, Extrasolar Planets: Today and Tomorrow, ed. J.-P. Beaulieu, A. Lecavelier des Etangs, & C. Terquem (San Francisco: ASP), 131
- Chabrier, G., & Baraffe, I. 2000, *ARA&A*, 38, 337
- Chabrier, G., Baraffe, I., Allard, F., & Hauschildt, P. 2000, *ApJ*, 542, 464
- Chauvin, G., Lagrange, A.-M., Dumas, C., Zuckerman, B., Mouillet, D., Song, I., Beuzit, J.-L., & Lowrance, P. 2004, *A&A*, 425, L29
- . 2005a, *A&A*, 438, L25
- Chauvin, G., et al. 2005b, *A&A*, 438, L29
- Chiang, E., & Murray-Clay, R. 2004, *ApJ*, 607, 913
- Close, L., et al. 2005, *Nature*, 433, 286
- Cushing, M., Rayner, J., Davis, S., & Vacca, W. 2003, *ApJ*, 582, 1066
- Cushing, M., Rayner, J., & Vacca, W. 2005, *ApJ*, 623, 1115
- Cutri, R., et al. 2003, 2MASS All-Sky Catalog of Point Sources
- Dahn, C., et al. 2002, *AJ*, 124, 1170
- Devillard, N. 1997, *Messenger*, 87, 19
- Dulick, M., Bauschlicher, C., Burrows, A., Sharp, C., Ram, R., & Bernath, P. 2003, *ApJ*, 594, 651
- Fortney, J., Marley, M., Hubickyj, O., Bodenheimer, P., & Lissauer, J. 2005, *Astron. Nachr.*, 326, 925
- Gizis, J. 2002, *ApJ*, 575, 484
- Gizis, J., & Bharat, R. 2004, *ApJ*, 608, L113
- Gizis, J., Riaz, B., & Hmiel, A. 2005a, *BAAS*, 37, 1338
- Gizis, J., Shipman, H., & Harvin, J. 2005b, *ApJ*, 630, L89
- Golimowski, D., et al. 2004, *AJ*, 127, 3516
- Herbst, W., et al. 2002, *PASP*, 114, 1167
- Herczeg, G., Wood, B., Linsky, J., Valent, J., & Johns-Krull, C. 2004, *ApJ*, 607, 369
- Jayawardhana, R., Ardila, D., Stelzer, B., & Haisch, K. E., Jr. 2003, *AJ*, 126, 1515
- Jayawardhana, R., Hartmann, L., Fazio, G., Fisher, R., Telesco, C., & Piña, R. 1999, *ApJ*, 521, L129
- Jayawardhana, R., Luhman, K., D'Alessio, P., & Stauffer, J. 2002, *ApJ*, 571, L51
- Kastner, J., Zuckerman, B., Weintraub, D., & Forveille, T. 1997, *Science*, 277, 67
- Kenyon, S., Brown, D., Tout, C., & Berlind, P. 1998, *AJ*, 115, 2491
- Kirkpatrick, D., Barman, T., Burgasser, A., McGovern, M. R., McLean, I. S., Tinney, C. G., & Lowrance, P. J. 2006, *ApJ*, 639, 1120
- Kirkpatrick, D., et al. 1999, *ApJ*, 519, 802
- Klein, R., Apai, D., Pascucci, I., Henning, Th., & Waters, L. 2003, *ApJ*, 593, L57
- Knacke, R., Fajardo-Acosta, S., & Tokunaga, A. 2004, *AJ*, 128, 2977
- Knapp, G., et al. 2004, *AJ*, 127, 3553
- Kraus, A., White, R., & Hillenbrand, L. 2005, *ApJ*, 633, 452
- . 2006, *ApJ*, 649, 306
- Kusakabe, N., et al. 2005, *ApJ*, 632, L139
- Lancon, A., & Rocca-Volmerange, B. 1992, *A&AS*, 96, 593
- Langhoff, S. R. 1997, *ApJ*, 481, 1007
- Leggett, S., Allard, F., Dahn, C., Hauschildt, P., Kerr, T., & Rayner, J. 2000, *ApJ*, 535, 965
- Leggett, S., Allard, F., Geballe, T., Hauschildt, P., & Schweitzer, A. 2001, *ApJ*, 548, 908
- Leggett, S., Hauschildt, P., Allard, F., Geballe, T., & Baron, E. 2002a, *MNRAS*, 332, 78
- Leggett, S., et al. 2002b, *ApJ*, 564, 452
- Liu, M., & Leggett, S. 2005, *ApJ*, 634, 616
- Liu, M., Najita, J., & Tokunaga, A. 2003, *ApJ*, 585, 372
- Lodato, G., Delgado-Donate, E., & Clarke, C. 2005, *MNRAS*, 364, L91
- Lucas, P., Roche, P., Allard, F., & Hauschildt, P. 2001, *MNRAS*, 326, 695
- Ludwig, H.-G. 2003, in IAU Symp. 210, Modelling of Stellar Atmospheres, ed. N. Piskunov, W. W. Weiss, & D. F. Gray (San Francisco: ASP), 113
- Ludwig, H.-G., Allard, F., & Hauschildt, P. 2006, *A&A*, 459, 599
- Luhman, K. 1999, *ApJ*, 525, 466
- . 2004, *ApJ*, 614, 398
- Luhman, K., Briceño, C., Stauffer, J., Hartmann, L., Barrado y Navascués, D., & Caldwell, N. 2003, *ApJ*, 590, 348
- Luhman, K., Liebert, J., & Rieke, G. 1997, *ApJ*, 489, L165
- Luhman, K., & Rieke, G. 1998, *ApJ*, 497, 354
- Luhman, K., Stauffer, J., & Mamajek, E. 2005, *ApJ*, 628, L69
- Mamajek, E. 2005, *ApJ*, 634, 1385
- Marley, M., Seager, S., Saumon, D., Lodders, K., Ackerman, A. S., Freedman, R. S., & Fan, X. 2002, *ApJ*, 568, 335
- Martín, E., Barrado y Navascués, D., Baraffe, I., Bouy, H., & Dahm, S. 2003, *ApJ*, 594, 525
- McLean, I., McGovern, M., Burgasser, A., Kirkpatrick, J., Prato, L., & Sungsoo, S. 2003, *ApJ*, 596, 561
- Mohanty, S., Basri, G., Jayawardhana, R., Allard, F., & Ardila, D. 2004a, *ApJ*, 609, 854
- Mohanty, S., Jayawardhana, R., & Barrado y Navascués, D. 2003, *ApJ*, 593, L109
- Mohanty, S., Jayawardhana, R., & Basri, G. 2004b, *ApJ*, 609, 885
- . 2005, *ApJ*, 626, 498
- Mohanty, S., Jayawardhana, R., Natta, A., Fujiyoshi, T., Motohide, T., & Barrado y Navascués, D. 2004c, *ApJ*, 609, L33
- Monin, J.-L., Clarke, C., Prato, L., & McCabe, C. 2006, in Protostars and Planets V, ed. B. Reipurth, D. Jewitt, & K. Keil (Tucson: Univ. Arizona Press), 395
- Monin, J.-L., Ménard, F., & Duchêne, G. 1998, *A&A*, 339, 113
- Muzerolle, J., Calvet, N., Briceño, C., Hartmann, L., & Hillenbrand, L. 2000, *ApJ*, 535, L47
- Padgett, D., Brandner, W., Stapelfeldt, K., Strom, S., Tereby, S., & Koerner, D. 1999, *AJ*, 117, 1490
- Partridge, H., & Schwenke, D. W. 1997, *J. Chem. Phys.*, 106, 4618
- Perryman, M., et al. 1997, *A&A*, 323, L49
- Phillips, J., Davis, S., Lindgren, B., & Balfour, W. 1987, *ApJS*, 65, 721
- Rubin, V., Burtley, J., Kiasatpoor, A., Klock, B., Pease, G., Rutscheidt, E., & Smith, C. 1962, *AJ*, 67, 491
- Scholz, A., & Jayawardhana, R. 2006, *ApJ*, 638, 1056
- Scholz, A., Jayawardhana, R., & Brandeker, A. 2005, *ApJ*, 629, L41
- Scholz, A., Jayawardhana, R., & Wood, K. 2006, *ApJ*, 645, 1498
- Schweitzer, A., Gizis, J. E., Hauschildt, P. H., Allard, F., Howard, E. M., & Kirkpatrick, J. D. 2002, *ApJ*, 566, 435
- Schweitzer, A., Gizis, J. E., Hauschildt, P. H., Allard, F., & Reid, I. N. 2001, *ApJ*, 555, 368
- Schwenke, D. W. 1998, *Faraday Discuss.*, 32(6), 27
- Ségransan, D., Kervella, P., Forveille, T., & Queloz, D. 2003, *A&A*, 397, L5
- Smith, V., et al. 2003, *ApJ*, 599, L107
- Solf, J. 1978, *A&AS*, 34, 409
- Song, I., Schneider, G., Zuckerman, B., Farihi, J., Becklin, E. E., Bessell, M. S., Lowrance, P., & Macintosh, B. A. 2006, *ApJ*, 652, 724
- Song, I., Zuckerman, B., & Bessell, M. 2003, *ApJ*, 599, 342
- Stapelfeldt, K., Krist, J., Ménard, F., Bouvier, J., Padgett, D., & Burrows, C. 1998, *ApJ*, 502, L65
- Stapelfeldt, K., et al. 1997, in IAU Symp. 182, Herbig Haro Flows and the Birth of Stars, ed. B. Reipurth & C. Bertout (Dordrecht: Kluwer), 355
- Stassun, K., Mathieu, R., & Valenti, J. 2006, *Nature*, 440, 311

- Stephens, D., & Leggett, S. 2004, PASP, 116, 9
Sterzik, M., Pascucci, I., Apai, D., van der Blieck, N., & Dullemond, C. 2004, A&A, 427, 245
Throop, H., Bally, J., Esposito, L., & McCaughrean, M. 2001, Science, 292, 1686
Torres, G., & Ribas, I. 2002, ApJ, 567, 1140
Vrba, F., et al. 2004, AJ, 127, 2948
Walker, C., Wood, K., Lada, C., Robitaille, T., Bjorkman, J., & Whitney, B. 2004, MNRAS, 351, 607
Wallace, L., & Hinkle, K. 2001, ApJ, 559, 424
Webb, R., Zuckerman, B., Platais, I., Patience, J., White, R. J., Schwartz, M. J., & McCarthy, C. 1999, ApJ, 512, L63
Weinberger, A., et al. 2002, ApJ, 566, 409
White, R., & Basri, G. 2003, ApJ, 582, 1109
Whitney, B., Kenyon, S., & Gómez, M. 1997, ApJ, 485, 703
Whitney, B., Wood, K., Bjorkman, J., & Cohen, M. 2003, ApJ, 598, 1079
Wichmann, R., Bastian, U., Krautter, J., Jankovics, I., & Rucinsky, S. 1998, MNRAS, 301, L39
Wing, R., & Ford, W. 1969, PASP, 81, 527
Winn, J., Holman, M., Johnson, J., Stanek, K., & Garnavich, P. 2004, ApJ, 603, L45
Zuckerman, B., & Song, I. 2004, ARA&A, 42, 685
Zuckerman, B., Webb, R., Schwartz, M., & Becklin, E. 2001, ApJ, 549, L233